UNIVERSITY OF CALIFORNIA
RIVERSIDE

Chemical and Physical Approaches to the Modulation of the Electronic Structure, Conductivities and Optical Properties of SWNT Thin Films

A Dissertation submitted in partial satisfaction
of the requirements for the degree of

Doctor of Philosophy

in

Chemistry

by

Matthew Lee Moser

December 2016

Dissertation Committee:
Dr. Eric Chronister, Chairperson
Dr. Vincent LaVallo
Dr. Mikhail Itkis

The Dissertation of Matthew Lee Moser is approved:

Committee Chairperson

University of California, Riverside

Acknowledgment

It was a great honor and privilege to work in the Haddon research group. It consists of the most dedicated, intelligent and friendly people I have ever met. The work included in this thesis would not have been possible without their teamwork and dedication.

I would like to thank my late advisor Professor Robert C. Haddon for the opportunity to research next generational carbon based electronics, a topic that fascinated me for years prior to the start of my graduate career. His guidance, tutorage and support were key to my success during these years of study. He will truly be missed. I would like to thank Misha Itkis. With great fondness I will most remember his willingness to share knowledge and guidance. He was someone I could turn to for anything. I will always consider him a mentor and a friend. I would like to thank Elena Bekyarova for her guidance and support. Her willingness to share knowledge will always be remembered and appreciated.

I would like to thank Aron Pekker for his patience, the knowledge he shared with me, the friendly advice and the help during our time together in the lab. His friendship is something I will always hold dear.

My success wouldn't have been possible without these fellow Haddon research group post docs and graduate students, Pradip Bag, Kumar Pal, Santanu Sarkar, Feihu Wang, Xiaojuan Tian, Mingguang Chen, Guanghui Li and Bassim Arkook. Thank you for the help and the great teamwork. I consider each one of you a friend and wish you all a successful future.

Special thanks to Dr. Eric Chronister for chairing my committee and reviewing my work and Dr. Vince LaVallo for taking the time to serve on my committee and also reviewing my work.

I wish to acknowledge the financial support from the Defense Microelectronics Activity (DMEA) under agreement number H94003-10-2-1003, the NSF under contracts DMR-1305724 and ECCS-1404671, and through the U.S. Department of Education GAANN award P200A120170.

Portions of the dissertation are adapted with permission from the following references:

Chapter 2: Moser, M. L.; Tian, X.; Pekker, A.; Sarkar, S.; Bekyarova, E.; Itkis, M. E.; Haddon, R. C., Hexahapto-Lanthanide Interconnects Between the Conjugated Surfaces of Single-Walled Carbon Nanotubes. *Dalton Trans.* **2014,** *43*, 7379-7382.

Chapter 3: Moser, M. L.; Pekker, A.; Tian, X.; Bekyarova, E.; Itkis, M. E.; Haddon, R. C., Effect of Lanthanide Metal Complexation on the Properties and Electronic Structure of Single-Walled Carbon Nanotube Films. *ACS Appl. Mat. & Interfaces* **2015,** *7*, 28013-28018.

Chapter 4: Moser, M.L.; Li, G.; Chen, M.; Bekyarova E.; Itkis M.E.; Haddon R.C., Fast Electrochromic Device Based on Single-Walled Carbon Nanotube Thin Films. *Nano Lett.* **2016**, 16, 5386-5393.

Dedication

I dedicate this thesis to my amazing children Peyton, Clara and Julie, to my loving parents and sisters and to my beautiful partner-in-crime and love of my life, Marilyn. All of your love and support made these pages possible.

ABSTRACT OF THE DISSERTATION

Chemical and Physical Approaches to the Modulation of the Electronic Structure, Conductivities and Optical Properties of SWNT Thin Films

by

Matthew Lee Moser

Doctor of Philosophy, Graduate Program in Chemistry
University of California, Riverside, December 2016
Dr. Eric Chronister, Chairperson

Since their discovery two decades ago, single walled carbon nanotubes (SWNT) have created an expansion of scientific interest that continues to grow to this day. This is due to a good balance between presence of bandgap, chemical reactivity and electrical conductivity. By interconnection of the individual nanotubes or modulation of the SWNT's electronic states, electronic devices made with thin films can become candidates for next generation electronics in areas such as memory devices, spintronics, energy storage devices and optoelectronics. My thesis focuses on the modulation of the electronic structure, optical properties and transport characteristics of single walled carbon nanotube films and their application in electronic and optoelectronic devices.

Individual SWNTs have exceptional electronic properties but are difficult to manipulate for use in electronic devices. Alternatively, devices utilize SWNTs in thin films. SWNT thin films, however, may lose some of the properties due to

Schottky barriers and electron hoping between metal-nanotube junctions and individual nanotubes within the film, respectively. Until recently, there has been no known route to preserve both conjugation and electrical properties. Prior attempts using covalent chemical functionalization led to re-hybridization of sp^2 carbon centers to sp^3, which introduces defects into the material and results in a decrease of electron mobility.

As was discovered in Haddon Research group, depositing Group VI transition metals via atomic vapor deposition into SWNT films results in formation of bis-hexahapto covalent bonds. This (η6–SWNT)Metal(η6–SWNT) type of bonding was found to interconnect the delocalized systems without inducing structural re-hybridization and results in a decrease of the thin films electrical resistance. Recently, with the assistance of electron beam deposition, we deposited atomic metal vapor of various lanthanide metals on the SWNT thin films with the idea that they would also form covalent interconnects between nanotube sidewalls. In the case of highly electropositive lanthanides, the possibility of hexahapto bonding combined with ionic character can be evaluated and theorized.

We have reported the first use of lanthanides to enhance the conductivities of SWNT thin films and showed that these metals can not only form bis-hexahapto interconnects at the SWNT junctions but can also inject electrons into the conduction bands of the SWNTs, forming a new type of mixed covalent-ionic bonding in the SWNT network. By monitoring electrical resistance and taking spectroscopic measurements of the Near-Infrared region we are able to show the

correlation between enhanced conductivity and suppression of the S_{11} interband transition of semiconducting SWNTs.

Potential applications of SWNT thin films as electrochromic windows require reversible modulation of the electronic structure. In order to fabricate SWNTs devices which allow for this behavior it is necessary to modulate the electronic structure by physical means such as the application of an electrical potential. We found that ionic solutions can assist with maintaining complete suppression of two Van Hove singularities in the Density of States of semiconducting SWNTs which results in optically transparent windows in the Near-Infrared region, similar to the effect seen with the incorporation of atomic lanthanide metals in thin films. We demonstrate this behavior to provide a route to nanotube based optoelectronic devices in which we use electric fields to reversibly dope the SWNT films and thereby achieve controllable modulation of optical properties of SWNT thin film.

Contents

Table of Figures

Chapter 1. Introduction

1.1 Introduction of Carbon Nanotubes

Conjugated carbon allotropes - fullerenes, carbon nanotubes (CNTs) and graphene - have been subjects of broad research interest due to their potential for novel applications spread across the scientific spectrum. Graphene largely considered the mother of all carbon allotropes can be shaped to form 0D fullerene or rolled to form 1D carbon nanotubes.(Figure 1.1) Carbon nanotubes come in many forms which vary by diameter and by the arrangement of their hexagonal arrays in the lattice. These differences result in changes to the density of electronic states and gives each type of carbon nanotube unique electrical and structural properties. Advances in synthesis and purification have given researchers access to higher quality materials which has enabled a better understanding of their unique properties and their promise for future electronic applications.

The discovery of the fullerenes in 1985[1] and the research that followed gave new insights into the properties of sp2 hybridized carbon allotropes. Less than a decade later at the NEC laboratory in Japan, Iijima's accidental discovery and analysis of multiwall carbon nanotubes (MWNT)(figure 1.2) focused scientific attention on the newest form of carbon materials.[2] The predicted 1D quantum effects for the electronic properties of CNT attracted the attention of researchers worldwide. Two years later single wall carbon nanotubes (SWNT) were

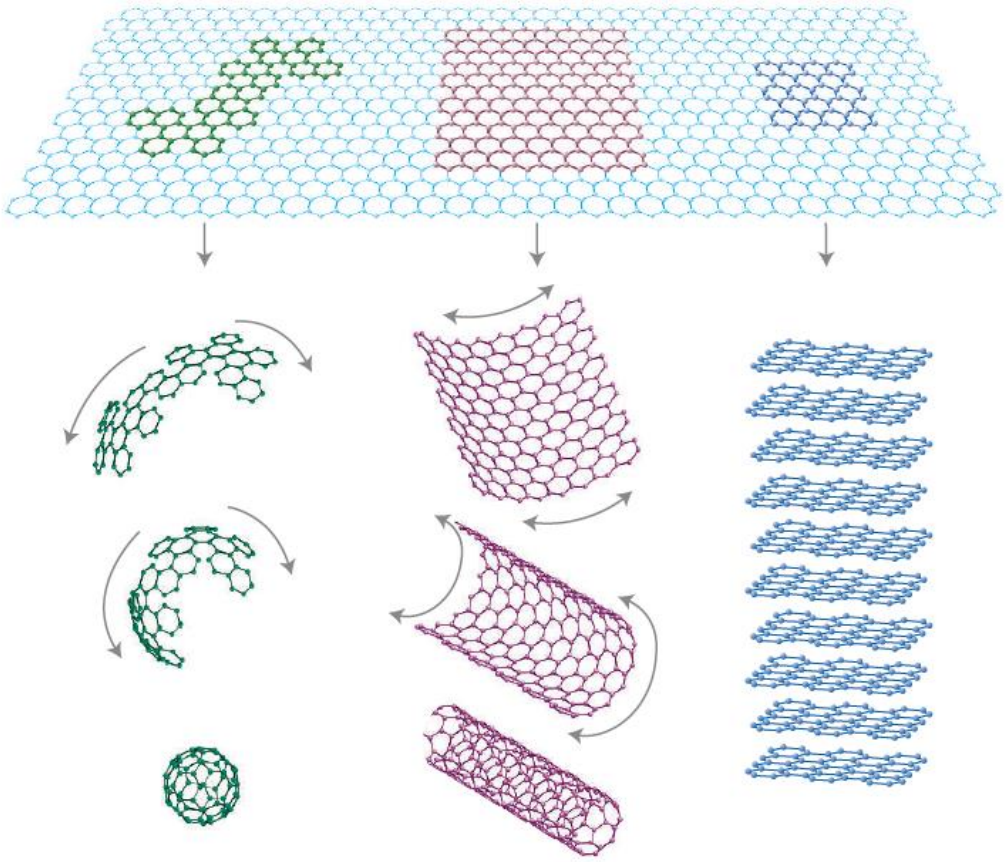

Figure 1.1 Graphene the mother of all carbon allotropes.[3]

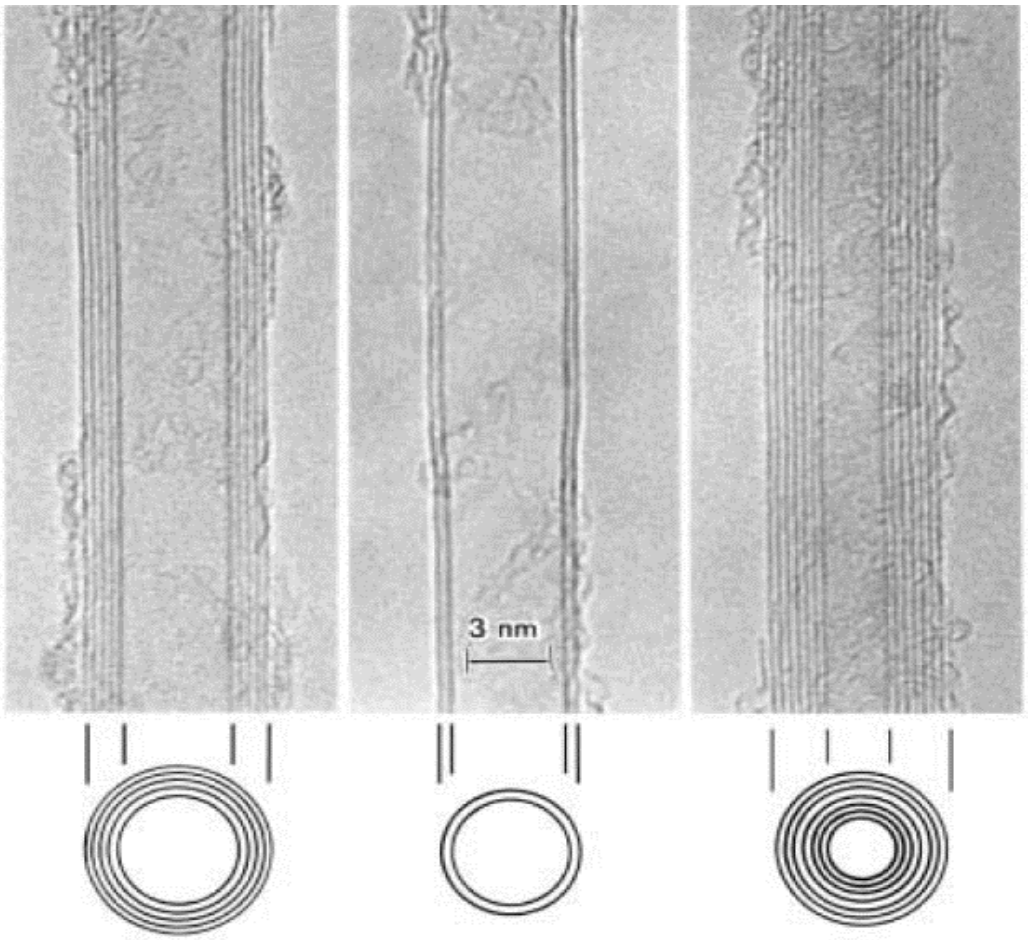

Figure 1.2 High resolution transmission electron microscopy (HR-TEM) image of MWNTs.[2]

synthesized [4, 5] and this created an expansion of scientific interest in the field that eventually grew to rival fullerene research.

1.2 Synthesis of Carbon Nanotubes

The synthesis of carbon nanotubes (CNTs) of different diameters, lengths and types (SWNTs, MWNTs) can be achieved by using specific methods and/or changing process parameters. Carbon nanotubes were first synthesized via electric arc (Figure 1.3)(EA),[4, 6] by passing high currents (50 A -100 A) through separated carbon electrodes in an inert atmosphere. The discharge of current creates a plasma arc which vaporizes the surface of anode while depositing product throughout the arc chamber and on the other electrode. This process makes bulk scale amounts of product, however, large CNT bundles and contaminants are formed during the process which requires purification to remove the byproducts and a separation process to unbundle CNT. Laser ablation (LA) uses laser pulses to vaporize graphite rods uniformly under an inert atmosphere.[6, 7] This method creates high quality nanotubes in low yields and scalability is an issue for the LA because of the need to maintain a uniform temperature in the reaction chamber. Chemical vapor deposition (CVD) can give large amounts of CNT,[8-10] but the method gives material with a high concentration of structural defects due to the low temperatures (500C-1000C) used in the process.

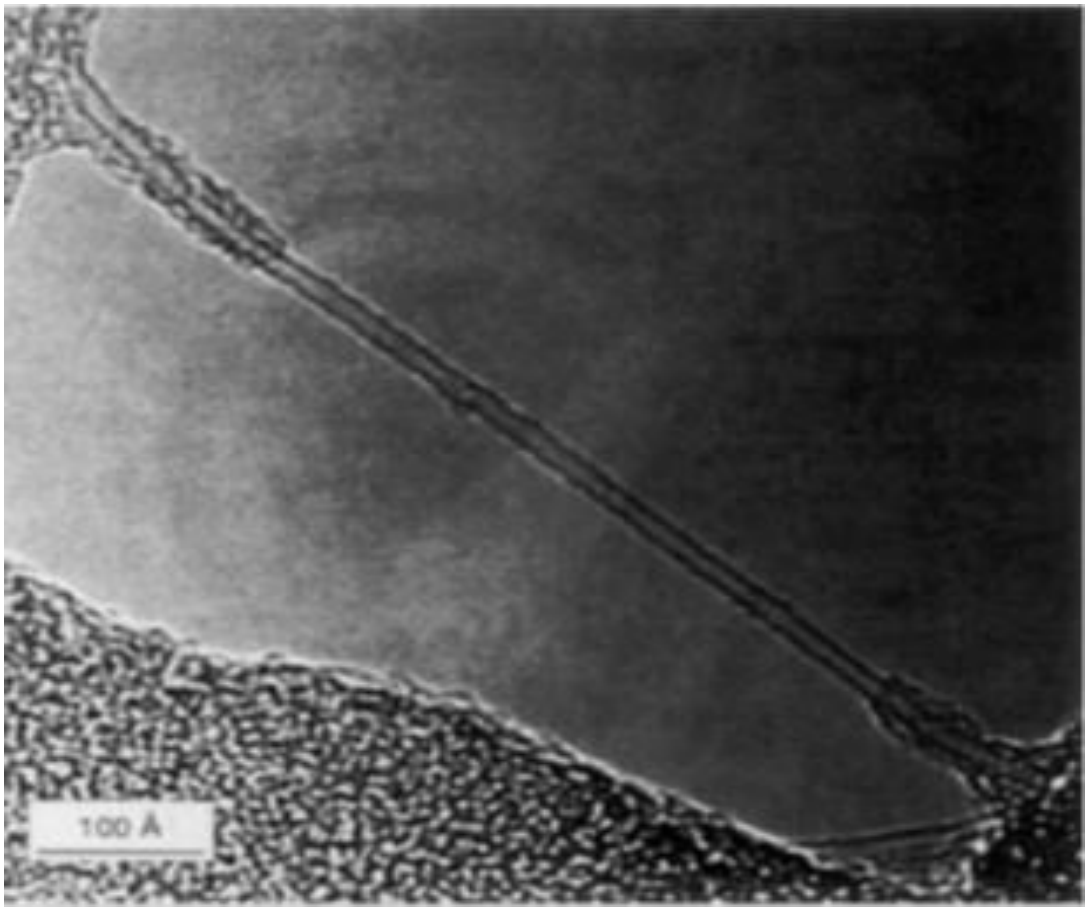

Figure 1.3 Arc discharge single-walled carbon nanotube (SWNTs) via transmission electron microscopy (TEM).[2]

1.3 Properties of Single Wall Carbon Nanotubes

If you imagine rolling a graphene sheet along the chiral vector $C_h = n\overrightarrow{a_1} + m\overrightarrow{a_2}$ the outcome would be identical to the seamless cylinder structure of a SWNT. The pair of integers (n, m) determine the structure of SWNT with chiral angle θ and unit vectors $\overrightarrow{a_1}$ and $\overrightarrow{a_2}$. (Figure 1.4) A graphene sheet that is rolled along the vector where θ=0° will form a zigzag nanotube. If θ=30° an armchair nanotube forms and for $0° < \theta < 30°$ this process forms chiral nanotubes. The diameter of the SWNT is given by $d = \sqrt{3}a_{c-c}\sqrt{n^2 + nm + m^2}$ where the carbon-carbon bond distance is $a_{c\text{-}c}$=0.142nm and the chiral angle follows from $\theta = tan^{-1}[\frac{\sqrt{3}n}{2m+n}]$. Armchair nanotube is characterized by values of m=n, while zigzag nanotubes have m=0 or n=0.

1.3.1 Electronic Properties of Single Wall Carbon Nanotubes

The pair of integers (n, m) not only determine the structure of SWNTs but also identifies the associated electronic structure. SWNTs and graphene are composed of conjugated sp^2 hybridized carbon, therefore the band structure theory of graphite can be applied to a SWNT in a simplified model. Graphene has a zero band gap because the valence and conduction bands touch at Dirac points. Rolling the graphene sheet along the chiral vector C_h forms a 1D tube, allowing the 1D subbands of SWNT to fulfill the periodic boundary conditions imposed by symmetry. The equation $C_h \cdot k = 2\pi q$ defines the quantized states where q is an

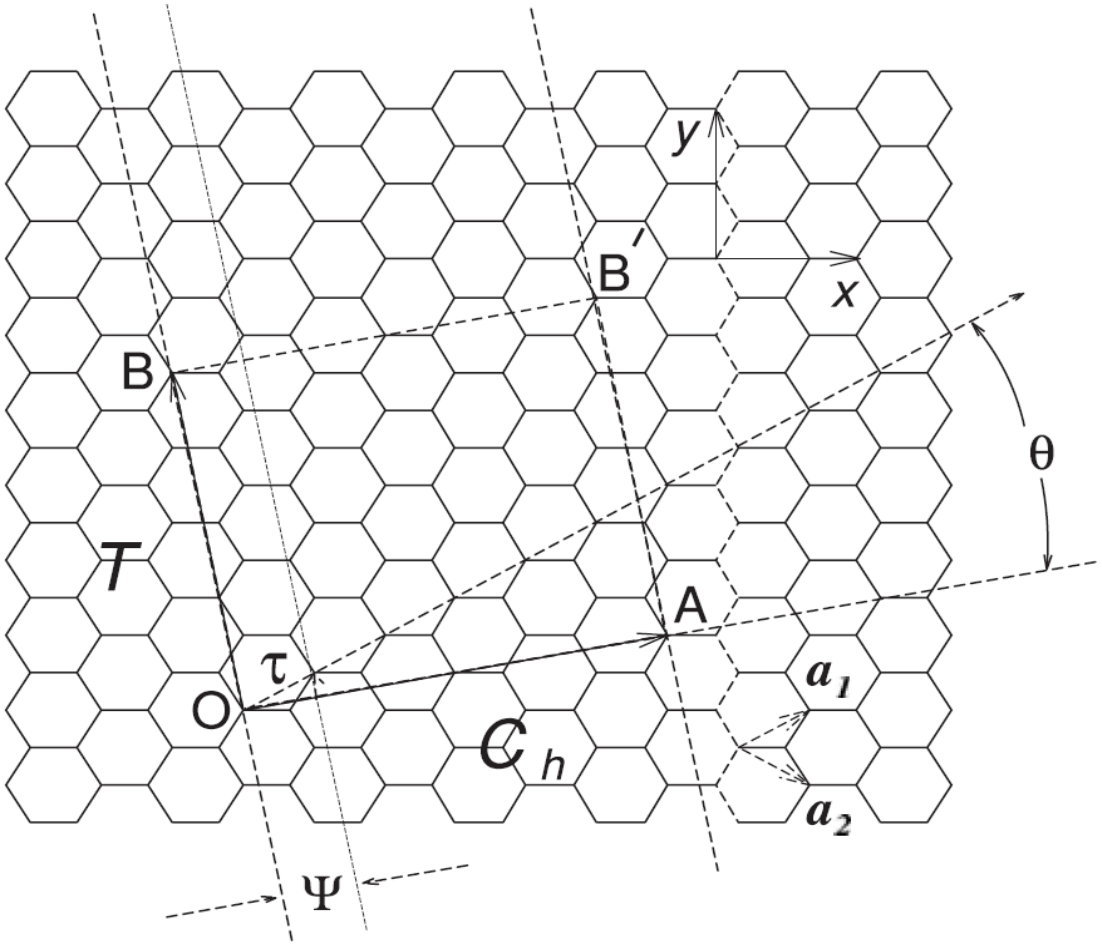

Figure 1.4 Chiral vector and chiral angle of SWNTs.[11]

integer and k is the quantized wavevector along the circumferential direction.(Figure 1.5)

If the subbands pass through one of the K points the SWNT is defined as metallic, such as armchair tubes (n.n). Chiral (n,m) SWNTs are metallic only if (n-m)/3 is an integer. All other SWNTs are semiconducting and the band gap is inversely proportional to the diameter.

In 1998 scanning tunneling spectroscopy experiments confirmed the presence and theoretical assignments of metallic and semiconducting SWNTs.[12, 13] Absorption spectroscopy is capable of observing the electronic transitions between the energy bands of SWNTs.[14-17]

SWNTs have extraordinary electrical properties, but must overcome a few challenges to reveal their total potential. Schottky barriers at the metal/nanotube interface limit overall performance significantly.[18] To combat this researchers used matching metals with ohmic contacts to decrease the energy of the Schottky barriers. It was found that carrier mobility reaches values around 10^5 $cm^2V^{-1}s^{-1}$ [19, 20] with ballistic transport conductance approaching quantum conductance $4e^2h^{-1}$.[21] Thin films networks of SWNTs have shown great promise for next generation electronic devices.[22-26] Thin films have conductivities around 250-400 S/cm which is about 100 times less the conductivity seen in individual nanotubes.[27] This decrease is due to nanotube-nanotube junctions found within the thin film, where

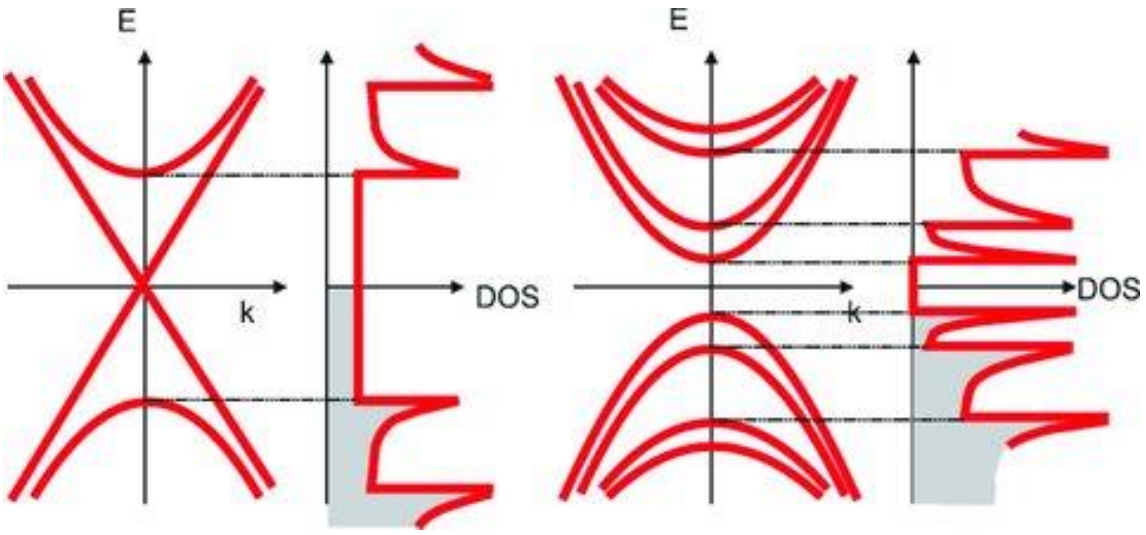

Figure 1.5 Band structure and density of states (DOS) of metallic SWNTs (left) and semiconducting SWNT (Right).[28]

electron mobility is determined by the energy requirement for electron hopping or tunneling between individual nanotubes.[29]

1.3.2 Optical Properties of Single Wall Carbon Nanotubes

Optical absorption bands corresponding to the energy gaps in electronic density of states of SWNTs can be found within the visible to mid infrared regions.(Figure 1.6) This makes absorption spectroscopy a convenient way to determine the electronic states of SWNTs. The electronic transitions in absorption spectra come from radial confinement of the wave function in SWNTs which produce specific energy levels in the density of states (DOS) called Van Hove singularities.[14-17] Optical absorption measurements can determine the level of chemical doping in nanotube systems due to Fermi level shifts into Van Hove singularities which result in suppression of the intensities of the interband transitions.[15]

1.3.3 Thermal and Mechanical Properties of Single Wall Carbon Nanotubes

The thermal conductivity of an individual SWNT can reach 6000 W/mK,[30] although the experimental values for SWNT thin films are much lower at 100 W/mK,[31] and 3000 W/mK for individual MWNTs.[32].

CNTs have outstanding mechanical properties. The CNTs tensile strength compared to steel is two orders of magnitude higher.[33] The calculated Young's modulus for an individual (10,10) SWNT is ~0.64 TPa and 1.47 TPa for a bundle

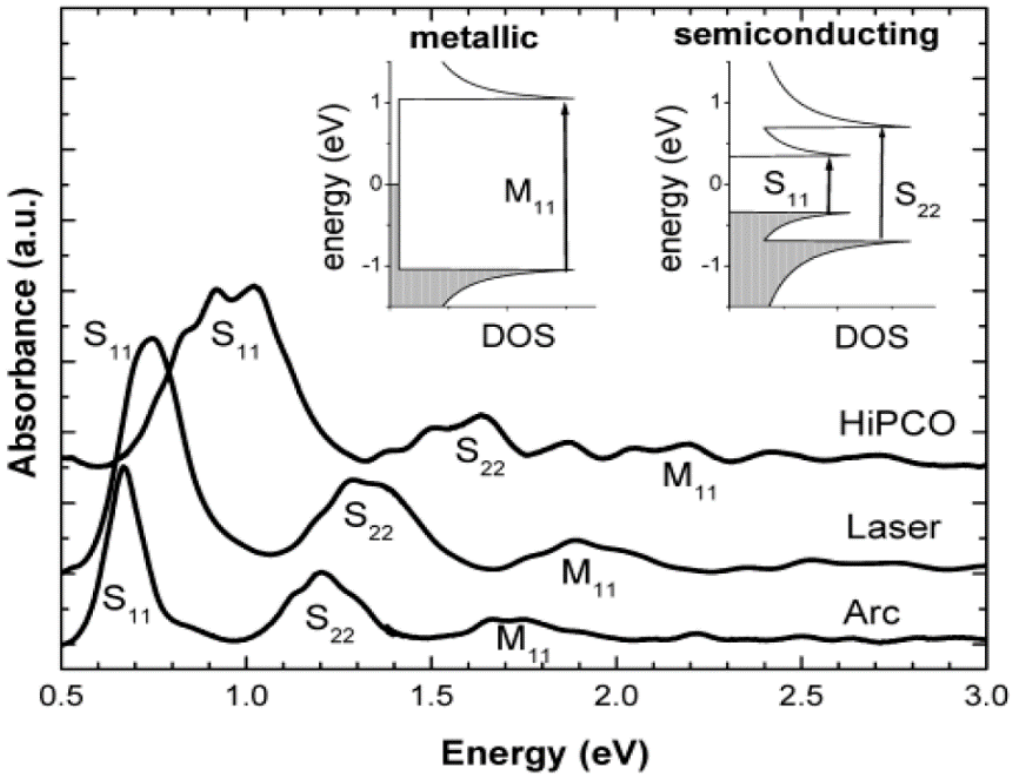

Figure 1.6 The absorption bands of SWNTs observed by spectroscopy confirmed the electronic transitions between the energy bands.[17]

of 15 SWNTs.[34] Measured Young's modulus of MWNTs is 1-2 TPa, and the bending strength of individual MWNTs is 28.5 GPa.[35, 36]

1.4 Chemical Reactivity of Carbon Nanotubes

The sp^2 bonding in carbon nanotubes makes the material quite stable, however, compared to graphene sheets the SWNT are more reactive due to local strains from curvature-induced pyramidalization and mis-alignment of the π-orbitals.[16, 37-43] The chemical reactivity of carbon nanotubes differs by region. Due to strain on the π-orbitals the carbon sites on end caps are more reactive than the sidewall carbon atoms.[17]

1.4.1 Dispersion of Bundles

Many characterization techniques and chemical reactions require the dissolution of the CNTs. In solid state they exist as bundles within the carbon lattices. The lack of surface functional groups on pure carbon SWNTs makes for difficulties to wet[44] or disperse the material in organic solvents,[37], due to their hydrophobic nature.

Dispersing SWNTs can be aided by nitric acid treatment. The oxidation reaction mainly takes place at the end caps. This reaction adds carboxylic acid and other weakly acidic functionalities to the carbon lattice.[45-47], Acid treated SWNTs can then be dispersed in organic solvent with relative ease.[48] Nitric acid

treatment also purifies the SWNTs of any remaining metal catalysts or amorphous carbon. Unfortunately, this procedure introduces defects at the nanotube walls.[49]

Another way to disperse SWNT is the addition of long-chain hydrocarbons at the ends. The acid functionality in SWNTs is converted to amide of octadecylamine (ODA).[14] The amide bond formation can be confirmed by mid-IR spectroscopy. The long-chain hydrocarbons are helpful to disrupt the van der Waals attraction in SWNT bundles. Bulky side chains can be added by various types of amide or ester bonds.[50-55]

1.5 Interactions Between Atomic Metal and SWNT Surfaces

There are two cases for interaction of metal with SWNT surfaces: the first involves single metal atoms and the second involves the bulk metal.[56, 57] I will only explain the former case which involves metal atoms added atomically to the graphitic surfaces by either physical or chemical methods. There are four known bonding interactions between individual metal atoms and SWNT surfaces.[57, 58] I describe these types of interactions in the following paragraphs.

1.5.1 Ionic Chemisorption

Metals with low ionization energies and low work functions inject electrons into the conduction band of SWNT (n-type doping (Figure 1.7)). Alkaline earth

(a) Covalent Chemisorption **(b) Ionic Chemisorption**

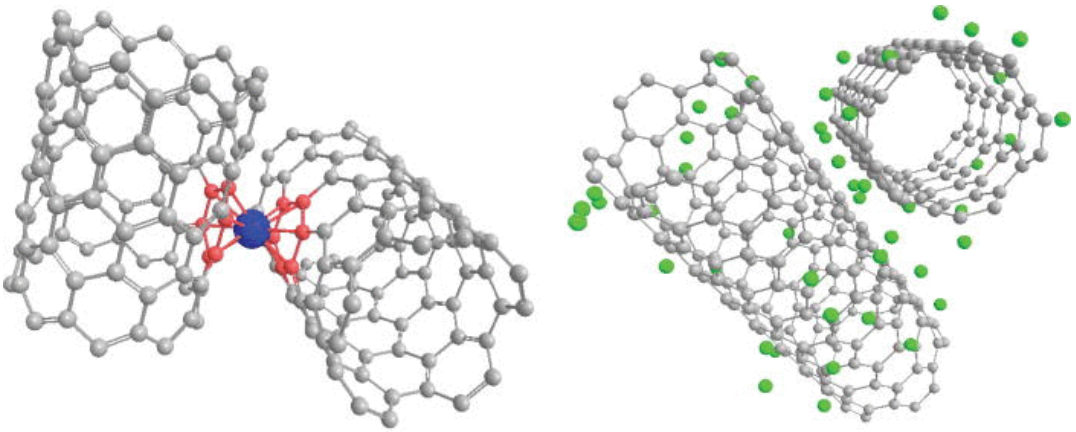

Figure 1.7 Enhancement of conductivity in semiconducting SWNT via ionic chemisorption (b), bis-hexahapto(η6) covalent chemisorption (a).[58]

metals (Ca, Sr, Ba) and alkali metals (Li, Na, K) interact by ionic chemisorption where charge transfer preserves the conjugation and band structure.

1.5.2 Covalent Chemisorption (destructive rehybridization)

Destructive covalent chemisorption of metals to the SWNT leads to rehybridization of the band structure. The formation of metal carbides is one such example where there is a strong interaction between the carbon atoms and metal. Covalent bond formation creates rehybridization of the carbon center to sp^3 and removes π-character from extended periodic π- electron structure from the system.[59]

1.5.3 Hexahapto(η6) Covalent Chemisorption (constructive rehybridization)

Constructive covalent chemisorption occurs in SWNT systems with metals capable of hexahapto(η6)−metal bond formation. This form of organometallic bonding preserves the graphitic band structure by preserving the extended periodic π- electron structure and maintains the delocalization on the SWNT surface. In nanotube thin films the constructive rehybridization leads to the formation of bis-hexahapto−metal bonds between two adjacent nanotubes, very similar to (η6 -SWNT)- Cr(η6 -SWNT) systems. This reduces electrical resistance caused by nanotube junctions in single-walled carbon nanotube (SWNT) networks by making interconnections between adjacent SWNTs, essentially giving electrons a lower energy pathway via an “atomic bridge” to the next nanotube.[58, 60-62]

1.5.4 Weak Physisorption

Metal atoms with filled d-orbitals (i.e. Au) or possessing a parabolic band structure with s,p-like metallic structure (i.e. Pb) add to SWNT thin films without significant effect to the band structure.[58]

1.6 Chemical and Physical Approaches to the Modulation of SWNT Thin Films Properties

1.6.1 Modulation of the Electronic Structure and Conductivities

The electronic properties of SWNT thin films can be fine-tuned to accommodate an applications specific need. Chemical doping is an easy way to increase conductivity of thin film networks[63] while covalent destructive rehybridization will decrease conductivity by creating an sp^3 carbon center defects within the nanotube lattice.[14, 64] However, when we deposit small amounts (1 < nm) of transition metals, we have seen an increase in SWNT thin film conductivity by 100x. (Figure 1.8) The η^6-bis-hexahapto bond that forms between benzenoid rings on adjacent carbon nanotubes to the d orbital electrons in metal atoms acts as an electron bridge between nanotubes.[62]

Lanthanide metals, once thought to exclusively form charge transfer complexes, can be used to provide rarer forms of conductivity enhancement. In Chapters 2 and 3, we report the first use of lanthanides to enhance the

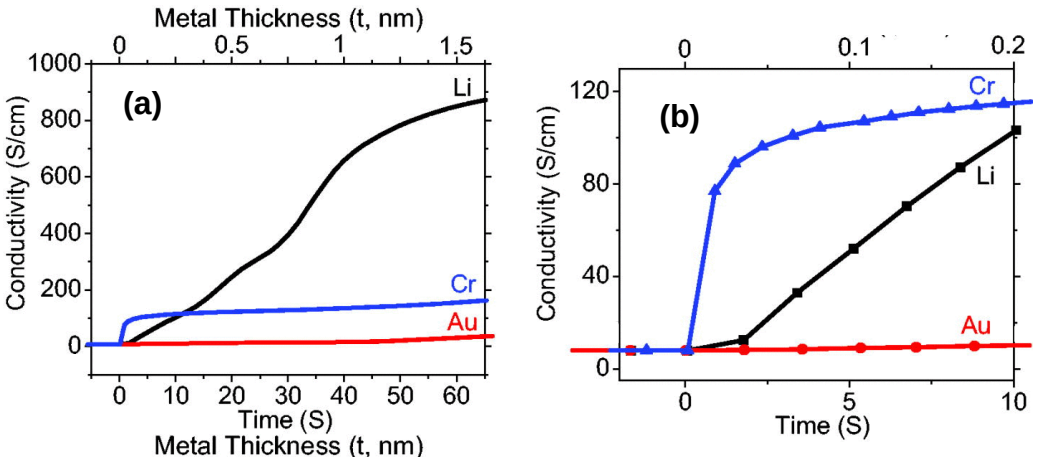

Figure 1.8 Enhancement of conductivity in semiconducting SWNTs via ionic chemisorption (Li), bis-hexahapto(η6) covalent chemsorption (Cr) and weak physisorption (Au).[58]

conductivities of SWNT thin films, and we show that these metals can not only form bis-hexahapto- interconnects at the SWNT junctions, but can also inject electrons into the conduction bands of the SWNTs and thereby form a newly discovered fifth mode of SWNT-Metal bonding called bis-hexahapto(η6) covalent chemisorption with Ionic character.

1.6.2 Modulation of the Optical Properties

Modulation of the optical properties in SWNT films can be achieved by chemical doping. Solution based doping of films using bromine completely suppressed the first two absorption bands, which made those regions transparent in the short wave infrared region.[37] Solid state doping using electron beam deposition to intercalate lithium metal into SWNT thin films also completely suppressed the low energy electronic transitions.[62]

Nanotube based optoelectronic devices using ionic liquid can achieve reversible doping by reversing electrical potential.[65] (Figure 1.9) We have shown that the modulation of the electronic structure of SWNT films can be achieved by covalent and ionic (doping) chemistry. In order to fabricate SWNT devices which show reversible behavior it is necessary to modulate the electronic structure by physical means such as the application of the electrical potential. Solution based doping can completely suppress features corresponding the transitions between first two pairs of Van Hove singularities in the DOS of the SWNTs, which make those regions transparent.[37, 66] In Chapter 4 we use this behavior to provide a route

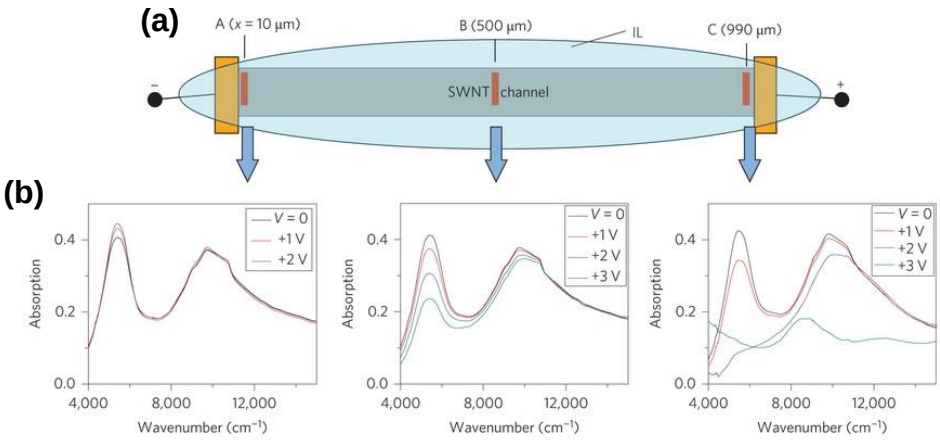

Figure 1.9 (a) SWNT electro-optical device. (b) SWNT absorption spectra modified by switching potential at either side.[65]

to nanotube based optoelectronic devices in which we use electric field to reversibly dope the SWNT films and thereby achieve controllable suppression of the electronic transitions,[65, 67, 68] thus opening new potential applications as electrochromic windows in which the electric field is used to modulate the short wave infrared light passing through the electrochromic cell.[69-71]

In this thesis, we explore the modulation of the electronic structure, transport and optical properties of SWNT thin films by the chemical addition of metal atoms to the SWNT surface,[58, 60, 61] and by the use of electrostatic and ionic liquid gating.[65]

References

1. Kroto, H. W.; Heath, J. R.; O'Brien, S. C.; Curl, R. F.; Smalley, R. E. *Nature* **1985,** 318, 162-164.

2. Iijima, S. *Nature* **1991,** 354, 56-58.

3. Geim, A. K.; Novoselov, K. S. *Nat. Mater.* **2007,** 6, 183-191.

4. Iijima, S.; Ichihashi, T. *Nature* **1993,** 363, 603-605.

5. Bethune, D. S.; Kiang, C. H.; de Vries, M. S.; Gorman, G.; Savoy, R.; Vazquez, J.; Bevers, R. *Nature* **1993,** 363, 605-607.

6. Journet, C.; Maser, W. K.; Bernier, P.; Loiseau, A.; Lamy de la Chappelle, M.; Lefrant, S.; Deniard, P.; Lee, R.; Fischer, J. E. *Nature* **1997,** 388, 756-758.

7. Guo, T.; Nikolaev, P.; Thess, A.; Colbert, D. T.; Smalley, R. E. *Chem. Phys. Lett.* **1995,** 243, 49-54.

8. Dai, H.; Rinzler, A. G.; Nikolaev, P.; Thess, A.; Colbert, D. T.; Smalley, R. E. *Chem. Phys. Lett.* **1996,** 260, 471-475.

9. Nikolaev, P.; Bronikowski, M. J.; Bradley, R. K.; Rohmund, F.; Colbert, D. T.; Smith, K. A.; Smalley, R. E. *Chem. Phys. Lett.* **1999,** 313, 91-97.

10. Joselevich, E.; Lieber, C. M. *Nano Lett.* **2002,** 2, 1137-1141.

11. Dresselhaus, M. S.; Dresselhaus, G.; Avouris, P., *Carbon Nanotubes: Synthesis, Structure, Properties and Applications*. Springer-Verlag: Berlin, 2001; Vol. 80.

12. Wildoer, J. W. G.; Venema, L. C.; Rinzler, A. G.; Smalley, R. E.; Dekker, C. *Nature (London)* **1998,** 391, 59-61.

13. Odom, T. W.; Huang, J.-L.; Kim, P.; Lieber, C. M. *Nature (London)* **1998,** 391, 62-64.

14. Chen, J.; Hamon, M. A.; Hu, H.; Chen, Y.; Rao, A. M.; Eklund, P. C.; Haddon, R. C. *Science* **1998,** 282, 95-98.

15. Itkis, M. E.; Niyogi, S.; Meng, M.; Hamon, M.; Hu, H.; Haddon, R. C. *Nano Lett.* **2002,** 2, 155-159.

16. Hamon, M. A.; Itkis, M. E.; Niyogi, S.; Alvaraez, T.; Kuper, C.; Menon, M.; Haddon, R. C. *J. Am. Chem. Soc.* **2001,** 123, 11292-11293.

17. Niyogi, S.; Hamon, M. A.; Hu, H.; Zhao, B.; Bhowmik, P.; Sen, R.; Itkis, M. E.; Haddon, R. C. *Acc. Chem. Res.* **2002,** 35, 1105-1113.

18. Appenzeller, J.; Knoch, J.; Derycke, V.; Martel, R.; Wind, S.; Avouris, P. *Phys. Rev. Lett.* **2002,** 89, 126801.

19. Dai, H. *Acc. Chem. Res.* **2002,** 35, 1035-1044.

20. Durkop, T.; Getty, S. A.; Cobas, E.; Fuhrer, M. S. *Nano Lett.* **2004,** 4, 35-39.

21. Javey, A.; Guo, J.; Wang, Q.; Lundstrom, M.; Dai, H. *Nature* **2003,** 424, 654-657.

22. Bradley, K.; Gabriel, J.-C. P.; Gruner, G. *Nano Lett.* **2003,** 3, 1353-1355.

23. Snow, E. S.; Campbell, P. M.; Ancona, M. G.; Novak, J. P. *Appl. Phys. Lett.* **2005,** 86, 033105.

24. Stadermann, M.; Papadakis, S. J.; Falvo, M. R.; Novak, J.; Snow, E.; Fu, Q.; Liu, J.; Fridman, Y.; Boland, J. J.; Superfine, R.; Washburn, S. *Phys Rev B* **2004,** 69, 201402.

25. Hu, L.; Hecht, D. S.; Gruner, G. *Nano Lett.* **2004,** 4, 2513-2517.

26. Kang, S. J.; Kocabas, C.; Ozel, T.; Shim, M.; Pimparkar, N.; Alam, M. A.; Rotkin, S. V.; Rogers, J. A. *Nature Nanotech.* **2007,** 2, 230.

27. Bekyarova, E.; Itkis, M. E.; Cabrera, N.; Zhao, B.; Yu, A.; Gao, J.; Haddon, R. C. *J. Am. Chem. Soc.* **2005,** 127, 5990-5995.

28. Nanot, S.; Haroz, E. H.; Kim, J. H.; Hauge, R. H.; Kono, J. *Adv Mater* **2012,** 24, 4977-94.

29. Hu, L. B.; Hecht, D. S.; Gruner, G. *Chem. Rev.* **2010,** 110, 5790-5844.

30. Hone, J.; Whitney, M.; Piskoti, C.; Zettl, A. *Phys Rev B* **1999,** 59, R2514-R2516.

31. Itkis, M. E.; Borondics, F.; Yu, A.; Haddon, R. C. *Nano Lett.* **2007,** 7, 900-904.

32. Kim, P.; Shi, L.; Majumdar, A.; McEuen, P. L. *Phys. Rev. Lett.* **2001,** 87, 215502.

33. Yakobson, B. I.; Smalley, R. E. *Am. Sci.* **1997,** 85, 324-337.

34. Gao, G.; Cagin, T.; Goddard III, W. A. *Nanotechnology* **1998,** 9, 184-191.

35. Treacy, M. M. J.; Ebbsen, T. W.; Gibson, J. M. *Nature* **1996,** 381, 678-680.

36. Wong, E. W.; Sheehan, P. E.; Lieber, C. M. *Science* **1997,** 277, 1971-1975.

37. Chen, Y.; Haddon, R. C.; Fang, S.; Rao, A. M.; Eklund, P. C.; Lee, W. H.; Dickey, E. C.; Grulke, E. A.; Pendergrass, J. C.; Chavan, A.; Haley, B. E.; Smalley, R. E. *J. Mater. Res.* **1998,** 13, 2423-2431.

38. Haddon, R. C. *Science* **1993,** 261, 1545-1550.

39. Haddon, R. C. *J. Am. Chem. Soc.* **1990,** 112, 3385-3389.

40. Scott, L. T.; Bratcher, M. S.; Hagen, S. *J. Am. Chem. Soc.,* **1996,** 118, 8743-8744.

41. Haddon, R. C.; Raghavachari, K. *Tetrahedron* **1996,** 52, 5207-5220.

42. Weedon, B. R.; Haddon, R. C.; Spielmann, H. P.; Meier, M. S. *J. Am. Chem. Soc.* **1999,** 121, 335-340.

43. Bodwell, G. J.; Bridson, J. N.; Houghton, T. J.; Kennedy, J. W. J.; Mannion, M. R. *Chem.-Eur. J.* **1999,** 5, 1823-1827.

44. Dujardin, E.; Ebbesen, T. W.; Krishnan, A.; Treacy, M. M. J. *Adv. Mater.* **1998,** 10, 1472-1475.

45. Ebbesen, T. W. *Acc. Chem. Res.* **1998,** 31, 558-566.

46. Mawhinney, D. B.; Naumenko, V.; Kuznetsova, A.; Yates, J. T. J.; Liu, J.; Smalley, R. E. *Chem. Phys. Lett.* **2000,** 324, 213-216.

47. Hu, H.; Bhowmik, P.; Zhao, B.; Hamon, M. A.; Itkis, M. E.; Haddon, R. C. *Chem. Phys. Lett.* **2001,** 345, 25-28.

48. Ausman, K. D.; Piner, R.; Lourie, O.; Ruoff, R. S.; Korobov, M. *J. Phys. Chem. B* **2000,** 104, 8911-8915.

49. Monthioux, M.; Smith, B. W.; Burteaux, B.; Claye, A.; Fischer, J. E.; Luzzi, D. E. *Carbon* **2001,** 39, 1251-1272.

50. Riggs, J. E.; Guo, Z.; Carroll, D. L.; Sun, Y.-P. *J. Am. Chem. Soc.* **2000,** 122, 5879-5880.

51. Sun, Y. P.; Huang, W.; Lin, Y.; Kefu, Y.; Kitaygorodskiy, A.; Riddle, L. A.; Yu, Y.; Caroll, D. L. *Chem. Mater.* **2001,** 13, 2864-2869.

52. Banerjee, S.; Wong, S. S. *Nano Lett.* **2002,** 2, 195.

53. Sano, M.; Kamino, A.; Okamura, J.; Shinkai, S. *Langmuir* **2001,** 17, 5125-5128.

54. Pompeo, F.; Resasco, D. E. *Nano Lett.* **2002,** 2, 369-373.

55. Basiuk, E. V.; Basiuk, V. A.; Banuelos, J.-G.; Saniger-Blesa, J.-M.; Pokrovskiy, V. A.; Gromovoy, T. Y.; Mischanchuk, A. V.; Mischanchuk, B. G. *J. Phys. Chem. B* **2002,** 106, 1588-1597.

56. Bekyarova, E.; Sarkar, S.; Wang, F.; Itkis, M. E.; Kalinina, I.; Tian, X.; Haddon, R. C. *Acc. Chem. Res.* **2013,** 46, 65-76.

57. Sarkar, S.; Moser, M. L.; Tian, X.; Zhang, X. J.; Al-Hadeethi, Y. F.; Haddon, R. C. *Chem. Mater.* **2014,** 26, 184-195.

58. Wang, F.; Itkis, M. E.; Bekyarova, E.; Tian, X.; Sarkar, S.; Pekker, A.; Kalinina, I.; Moser, M.; Haddon, R. C. *Appl. Phys. Lett.* **2012,** 100, 223111.

59. Sarkar, S.; Bekyarova, E.; Haddon, R. C. *Mater. Today* **2012,** 15, 276-285.

60. Kalinina, I.; Bekyarova, E.; Sarkar, S.; Wang, F.; Itkis, M. E.; Tian, X.; Niyogi, S.; Jha, N.; Haddon, R. C. *Macromol. Chem. Phys.* **2012,** 213, 1001-1019.

61. Wang, F.; Itkis, M. E.; Bekyarova, E.; Sarkar, S.; Tian, X.; Haddon, R. C. *J. Phys. Org. Chem.* **2012,** 25, 607-610.

62. Tian, X.; Moser, M. L.; Pekker, A.; Sarkar, S.; Ramirez, J.; Bekyarova, E.; Itkis, M. E.; Haddon, R. C. *Nano Lett.* **2014,** 14, 3930-3937.

63. Lee, R. S.; Kim, H. J.; Fischer, J. E.; Thess, A.; Smalley, R. E. *Nature* **1997,** 388, 255-257.

64. Boul, P. J.; Liu, J.; Mickelson, E. T.; Huffman, C. B.; Ericson, L. M.; Chiang, I. W.; Smith, K. A.; Colbert, D. T.; Hauge, R. H.; Margrave, J. L.; Smalley, R. E. *Chem. Phys. Lett.* **1999,** 310, 367-372.

65. Wang, F.; Itkis, M. E.; Bekyarova, E.; Haddon, R. C. *Nature Photon.* **2013,** 7, 459-465.

66. Wu, Z.; Chen, Z.; Du, X.; Logan, J. M.; Sippel, J.; Nikolou, M.; Kamaras, K.; Reynolds, J. R.; Tanner, D. B.; Hebard, A. F.; Rinzler, A. G. *Science* **2004,** 305, 1273-1276.

67. Cho, S. I.; Kwon, W. J.; Choi, S.-J.; Kim, P.; Park, S.-A.; Kim, J.; Son, S. J.; Xiao, R.; Kim, S.-H.; Lee, S. B. *Adv. Mater.* **2005,** 17, 171-175.

68. Yanagi, K.; Moriya, R.; Yomogida, Y.; Takenobu, T.; Naitoh, Y.; Ishida, T.; Kataura, H.; Matsuda, K.; Maniwa, Y. *Adv. Mater.* **2011,** 23, 2811-2814.

69. Baetens, R.; Jelle, B. P.; Gustavsen, A. *Sol. Energ. Mat. Sol. Cells* **2010,** 94, 87-105.

70. Granqvist, C. G. *Thin Solid Films* **2014,** 564, 1-38.

71. Mortimer, R. J.; Rosseinsky, D. R.; Monk, P. M. S. e., *Electrochromic Materials and Devices*. Wiley-VCN Verlag GmbH & Co. KGaA: Veinheim, Germany, 2013.

Chapter 2. Lanthanide SWNT Bis-Hexahapto Complexes as First Examples of a Mixed Covalent–Ionic Bis-Hexahapto Bonds.

2.1 Introduction

The conjugated carbon allotropes – fullerenes, carbon nanotubes and graphene – exist as continuous arrays of trivalent carbon atoms. There is no simple route to their covalent interconnection which preserves the conjugation; thus the interconnection of benzenoid surfaces is an important problem in the realization of carbon electronics. We have recently introduced the use of organometallic hexahapto covalent bonding of transition metals to graphene surfaces in order to interconnect such delocalized systems without inducing structural re-hybridization.[1] This new type of bonding is able to interconnect single-walled carbon nanotubes (SWNTs) and decreases the electrical resistance of thin film networks, particularly on formation of the (η^6–SWNT)Cr(η^6–SWNT) bond. While such bonds are expected to be covalent, the use of the highly electropositive lanthanides offers the possibility of hexahapto bonding combined with ionic character. In the present manuscript we report the electrical response of semiconducting (SC–) SWNT films on exposure to metal vapors of the early lanthanides (Ln) under high vacuum conditions and we show that there is a strong increase in the conductivity associated with all metals but only samarium (Sm) and europium (Eu) exceed the previously determined values of the first row transition

metals. We suggest that the enhanced conductivities shown by Sm and Eu is due to charge transfer from metal to the SWNT backbone, thereby leading to the first examples of a mixed covalent–ionic bis-hexahapto bond.

The metal vapor synthesis (MVS) technique[2] has proved to be an extremely versatile method for the preparation of neutral organometallic complexes.[3, 4] The use of the electron-gun furnace (or e-beam),[5, 6] greatly expanded the range of evaporable metals and allowed the isolation of the first zerovalent bis-hexahapto-arene-lanthanide complexes [Ln(η^6-arene)$_2$].[7, 8] We have shown that e-beam evaporation of very small amounts of transition metals on thin films of SWNTs under high vacuum conditions significantly enhances their conductivity.[1, 9, 10] It is well known that the nanotube junctions are the principle source of electrical resistance in such networks,[11-13] and given the known mobility of transition metals on graphitic surfaces and the geometric and electronic requirements for bis-hexahapto bond formation it is apparent that these nanotube complexes [M[(η^6-SWNT)$_2$, where M = transition metal] form spontaneously at the network junctions[1] in analogy with the low temperature reactions observed in the MVS experiments.[2-6]

An interesting outcome of the carbon nanotube studies is the finding that chromium gives rise to the highest conductivities,[9] in apparent validation of the 18 electron rule of organometallic chemistry.[14] We had expected that bis-hexahapto-metal bonds, which deviate from the 18 electron rule, might be associated with enhanced conductivities due to the accessibility of electronic configurations

involving charge transfer, but in the cases examined to date there is no evidence for this type of bonding.[1, 9, 10] We explore the behavior of the early lanthanides and we report results suggesting that selected members of this series are able to access mixed covalent-ionic bonding when allowed to interact with the graphene surfaces of SWNTs under high vacuum conditions.

2.2 Experimental

The metal deposition experiments were performed on 8 nm thick films of semiconducting (SC-) SWNTs. The films were prepared on an alumina membrane disk by vacuum filtration and sliced into 4 mm x 2 mm rectangles, which were mounted on substrates with gold contacts via silver paste (Figure 2.1).[9] After annealing at 573 K for 3 hours, the substrates were transferred into a cryo-pumped Temescal BJD 1800 e-beam evaporator equipped with custom fittings to allow the measurement of the *in-situ* film resistance. The conductivity (σ) of the pristine SC-SWNT films was σ = 2 S/cm.

In each set of experiments the metal was deposited continuously on the carbon nanotube films until a thickness of 2 nm was obtained.[9, 15] It is important to note that the deposition of 2 nm of lanthanide metals on a blank channel without a SWNT film did not result in a measurable conductance (R > 100 Mohm), thereby indicating that this amount of deposited metal is not sufficient to form a continuous conducting metal film.

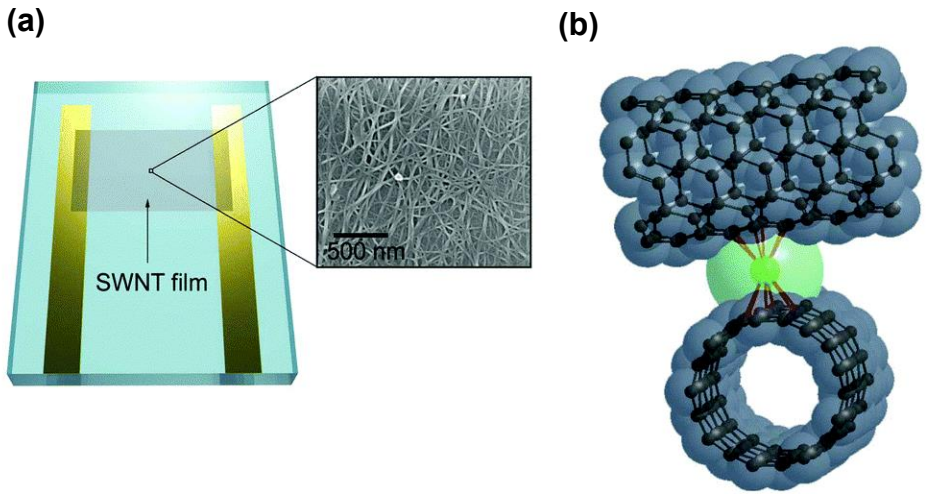

Figure 2.1 Network of single-walled carbon nanotubes (SWNTs) and the bonding of a lanthanide atom at a SWNT junction. a, SWNT film mounted on gold contacts for e-beam deposition of lanthanides; inset shows an SEM image of SWNT film. b, schematic of two SWNTs bridged by a lanthanide atom.

2.3 Results and Discussion

Figure 2.2 displays the conductivity of SC-SWNT films during atomic vapor deposition of lanthanum (La), neodymium (Nd), samarium (Sm), europium (Eu), and gadolinium (Gd) and it is apparent that all of the metals elicit a strong response in the film conductivities. The first point of interest is the stability of the bis-hexahapto-lanthanide complexes: whereas Nd and Gd form isolable complexes with 1,3,5-tri-t-butylbenzene (Bz*) of formula [Ln(η^6-Bz*)$_2$],[8, 16] the other metal complexes showed the following degradation temperatures: Eu (200 K), Sm (225 K), and La (273 K).[8, 16] Similarly, experimental estimates of the mean metal-arene bond enthalpies [*D*(M-arene) for the process M(η^6- arene)$_2$ $\rightarrow$ M° + 2 arene] indicate values of 32 kcal/mol (Eu), 37 (Sm), 57 (Nd), 69 (La), and 69 (Gd).[17] Our experiments show that all of the Ln(η^6-SWNT)$_2$ complexes are thermally stable in high vacuum and heating the samples to 400 K did not degrade the materials as evidenced by the electrical conductivities.

Based on a frontier molecular orbital treatment of the electronic structure of graphene at the Dirac point we have suggested that graphene and SWNTs should be excellent ligands for hexa-hapto-transition metal complexes,[1, 18] in agreement with the present findings. The previous results obtained on Cr are included in Figure 2.2 for comparison and it is apparent that the conductivity enhancements shown by the lanthanides fall into two groups, one of which includes metals that

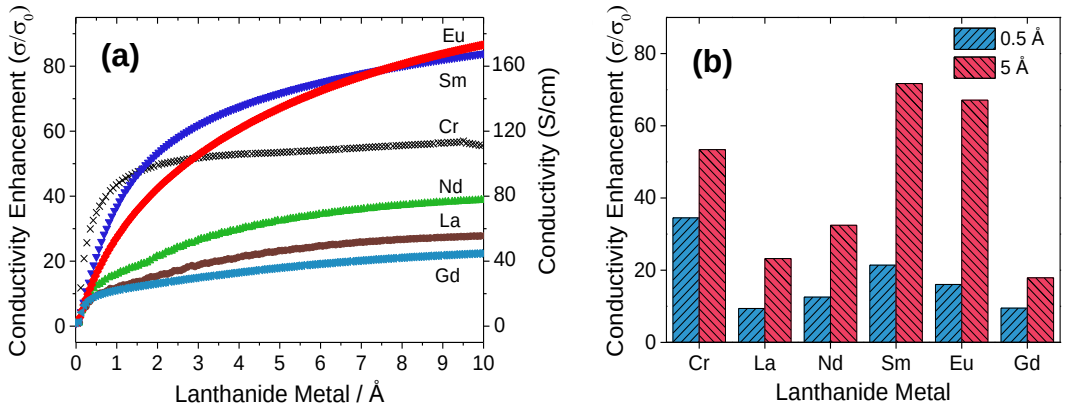

Figure 2.2 Effect of lanthanide deposition on the conductivities of SC-SWNT films. a, Conductivity enhancement of semiconducting single-walled carbon nanotube (SC-SWNT) films of thickness, t = 8nm, as a function of metal deposition. b, Conductivity enhancement of SC-SWNT films after the deposition of 0.5 Å and 5 Å of lanthanide metal.

exceed the conductivities shown by the transition metals studied to date.[9, 10] The rapid saturation of the conductivity in the case of Cr is attributed to the knetically favorable formation of the (η^6–SWNT)Cr(η^6–SWNT) bond.[1, 9]

The electronic structure of the Ln(η^6-arene) and Ln(η^6-arene)$_2$ complexes have received detailed experimental and theoretical examination[8, 16, 17, 19-22] and the most widely accepted model for hexa-hapto-lanthanide complexation relies on the generation of the $5d^1\,6s^2$ electronic configuration at the metal center thereby requiring a consideration of the $4f^n\,6s^2 \rightarrow 4f^{n-1}\,5d^1\,6s^2$ promotion energy.[8, 19, 20] In Figure 2.3 we have plotted the conductivity enhancements as a function of the $4f^n\,6s^2 \rightarrow 4f^{n-1}\,5d^1\,6s^2$ transition energies and it may be seen that there is an excellent correlation; thus Sm and Eu require about 2 eV to produce the requisite electronic structure for bis-hexahapto bonding and on this basis we have generated the orbital interaction diagram for Eu and Gd shown in Figure 2.4.

There are uncertainties associated with the construction of this orbital correlation diagram but as much as possible we have followed the previous literature regarding the electronic structure of lanthanide complexes,[8, 16, 17, 19-25] theoretical analyses of organometallic bonding to SWNTs and graphene,[26-28] and frontier molecular orbital theory.[1] We have closed the gap between the highest occupied and lowest unoccupied arene molecular orbitals (HOMO and LUMO, respectively) in Figure 2.4, in recognition of the small energy gap between the valence and conduction bands of SC-SWNTs,[29] while retaining the usual arene

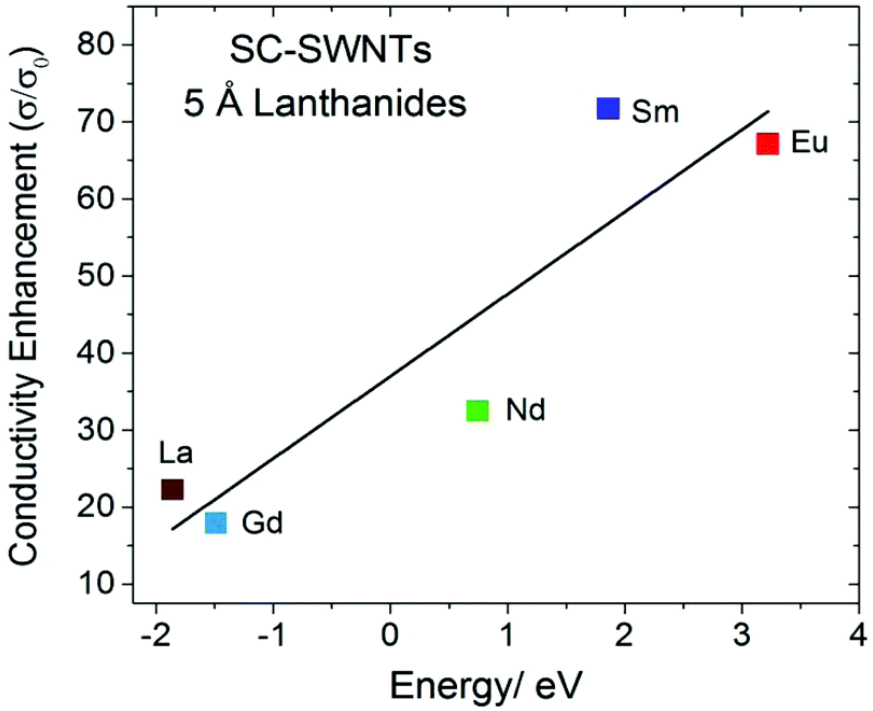

Figure 2.3 Enhancement of carbon nanotube conductivity as a function of the $4f^n$ $6s^2 \rightarrow 4f^{n-1}$ $5d^1$ $6s^2$ transition energies of the lanthanides. Conductivity enhancement of SC-SWNT films of 8 nm thickness after deposition of 5 Å La, Gd, Nd, Sm and Eu; the conductivity values are given relative to the initial conductivity (σ_0) of the pristine SC-SWNT film.

symmetry labels, which are expected to correlate with the symmetries of the SWNT bands at selected points in momentum space.[1]

The orbital energy correlation diagram for gadolinium is standard for the Ln(η^6-benzene)$_2$ complexes;[8, 16, 17, 19-22] in the case of Gd(η^6-benzene)$_2$ there are two low energy metal states: $^9E_{2g}$ ($4f^7 5d^3$ Gd configuration) and $^{11}A_{2g}$ ($4f^7 5d^2 4s^1$ Gd), with $^9E_{2g}$ as the likely ground state.[19, 20] The half-filled 4f orbitals remain completely localized on the metal atoms and will not be considered further; thus the bonding is principally dependent on the interaction of the arene π-orbitals and metal 5d orbitals. In the present case the L (ligand) $\rightarrow$ M (metal) component comprises the a_{1g} SWNT π-orbitals which lie near the bottom of the valence band (VB) and the 5d and 6s metal orbitals of the same symmetry, but the more important contribution originates from the e_{1g} interaction between the metal d_{XZ}, d_{YZ} orbitals and the SWNT π-orbitals which lie near the top of the VB and are well positioned to interact strongly with the metal.[1, 10]

The reverse electron donation involving the M $\rightarrow$ L interaction is at least as important as the L $\rightarrow$ M component of the bonding,[8, 16, 17, 19-22] and in the present case takes on particular significance.

The low lying conduction band (CB) of the SWNTs suggests that the electropositive nature of the lanthanides will allow the $5d_{XY}$, $5d_{X2-Y2}$ orbitals to make a very strong donation of electron density into the e_{2g} orbitals near the bottom of the CB of the SWNTs. We further suggest that in case of Eu and Sm, because of the high promotion energy associated with the valence $5d^1 6s^2$ configuration of the

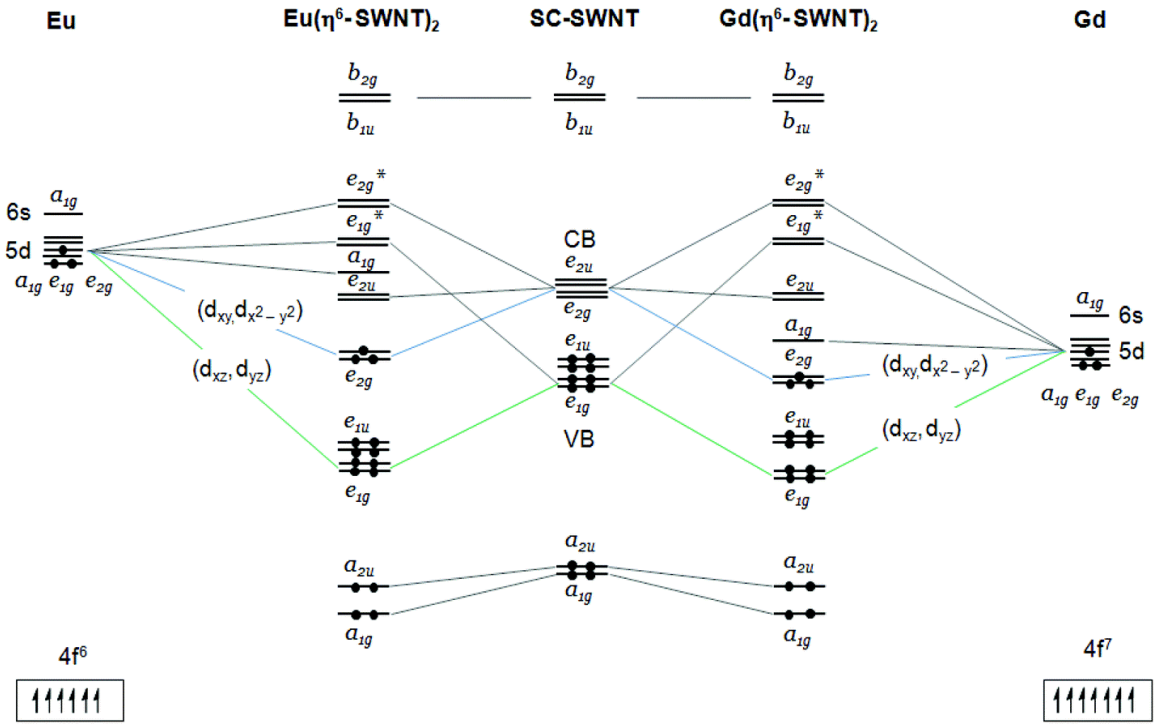

Figure 2.4 Orbital correlation diagram for the interaction of the semiconducting single-walled carbon nanotube (SC-SWNT) ligands with gadolinium (Gd) and Europium (Eu). The schematic diagram includes those orbitals which are germane to the present discussion; complete, quantitative treatments of orbital energy levels of the M(η6-arene)2 complexes, where M = transition metal and lanthanide and arene = benzene, SWNT, and graphene fragment are available in the literature.[17, 20-22, 26, 27]

metal, the 5d orbitals will be moved up in energy to the point that electrons are released into the CB of the SC-SWNTs. This electronic structure rationalizes the large conductivity difference between Gd and Eu and the fact that the conductivities of Eu and Sm exceed those of all other lanthanides and transition metals examined to date. Given the tendency of the electropositive lanthanides to form the trivalent and divalent oxidation states[30-33] it is reasonable to assume that ionic bonding should be relevant in members of this series.

2.4 Conclusion

The stability of the Ln(η^6-SWNT)$_2$ complexes establishes the graphitic surfaces of the SWNTs as excellent ligands in bis-hexahapto coordination compounds and the conductivity of the M(η^6-arene)$_2$ bond highlights the ability of this linkage to seamlessly interconnect the conjugated surface of SWNTs and graphene to extend their dimensionality. The strongly enhanced conductivity of Sm(η^6-SWNT)$_2$ and Eu(η^6-SWNT)$_2$ supports the idea that these complexes exhibit the first instances of mixed covalent-ionic bonding in bis-hexahapto-metal complexes.

References

1. Bekyarova, E.; Sarkar, S.; Wang, F.; Itkis, M. E.; Kalinina, I.; Tian, X.; Haddon, R. C. *Acc. Chem. Res.* **2013,** 46, 65-76.

2. Timms, P. L. *Chem. Commun.* **1969**, 1033.

3. Timms, P. L. *Adv. Inorg. Chem. Radiochem.* **1972,** 14, 121-171.

4. Pampaloni, G. *Coord. Chem. Rev.* **2010,** 254, 402-419.

5. Benfield, F. W. S.; Green, M. L. H.; Ogden, J. S.; Young, D. *J. Chem. Soc., Chem. Commun.* **1973**, 866-867.

6. Green, M. L. H. *J. Organomet. Chem.* **1980,** 200, 119-132.

7. Brennan, J. F.; Cloke, F. G. N.; Sameh, A. A.; Zalkin, A. *J. Chem. Soc., Chem. Commun.* **1987**, 1668-1669.

8. Cloke, F. G. N. *Chem. Soc. Rev.* **1993**, 17-24.

9. Wang, F.; Itkis, M. E.; Bekyarova, E.; Tian, X.; Sarkar, S.; Pekker, A.; Kalinina, I.; Moser, M.; Haddon, R. C. *Appl. Phys. Lett.* **2012,** 100, 223111.

10. Kalinina, I.; Bekyarova, E.; Sarkar, S.; Wang, F.; Itkis, M. E.; Tian, X.; Niyogi, S.; Jha, N.; Haddon, R. C. *Macromol. Chem. Phys.* **2012,** 213, 1001-1019.

11. Bekyarova, E.; Itkis, M. E.; Cabrera, N.; Zhao, B.; Yu, A.; Gao, J.; Haddon, R. C. *J. Am. Chem. Soc.* **2005,** 127, 5990-5995.

12. De, S.; King, P. J.; Lyons, P. E.; Khan, U.; Coleman, J. N. *ACS Nano* **2010,** 4, 7064.

13. Hu, L. B.; Hecht, D. S.; Gruner, G. *Chem. Rev.* **2010,** 110, 5790-5844.

14. Elschenbroich, C., *Organometallics*. Third ed.; Wiley-VCH: Weinheim, 2006.

15. Wang, F.; Itkis, M. E.; Bekyarova, E.; Sarkar, S.; Tian, X.; Haddon, R. C. *J. Phys. Org. Chem.* **2012,** 25, 607-610.

16. Arnold, P. A.; Petrukhina, M. A.; Bochenov, V. E.; Shabatina, T. I.; Zagorskii, V. V.; Sergeev, G. B.; Cloke, F. G. N. *J. Organometal. Chem.* **2003,** 688, 49-55.

17. King, W. A.; Di Bella, S.; Lanza, G.; Khan, K.; Duncalf, D. J.; Cloke, F. G. N.; Fragala, I. L.; Marks, T. J. *J. Am. Chem. Soc.* **1996,** 118, 627-635.

18. Sarkar, S.; Bekyarova, E.; Haddon, R. C. *Acc. Chem. Res.* **2012,** 45, 673-682.

19. Anderson, D. M.; Cloke, F. G. N.; Cox, P. A.; Edelstein, N.; Green, J. C.; Tanya Pang ; Sameh, A. A.; Shalimoff, G. *J. Chem. Soc., Chem. Commun.* **1989**, 53-55.

20. Di Bella, S.; Lanza, G.; Fragala, I. L.; Marks, T. J. *Organometallics* **1996,** 15, 3985-3989.

21. Hong, G.; Schautz, F.; Dolg, M. *J. Am. Chem. Soc.* **1999,** 121, 1502-1512.

22. Roudjane, M.; Kumari, S.; Yang, D.-S. *J. Phys. Chem. A* **2012,** 116, 839-845.

23. Citrin, P. H.; Ozdas, E.; Schuppler, S.; Kortan, A. R.; Lyons, K. B. *Phys. Rev. B.* **1997,** 56, 5213-5227.

24. Chen, X. H.; Roth, G. *Phys Rev B* **1995,** 52, 15534-15536.

25. Ginwalla, A. S.; Balch, A. L.; Kauzlarich, S. M.; Irons, S. H.; Klavins, P.; Shelton, R. N. *Chem. Mater.* **1997,** 9, 278-284.

26. Avdoshenko, S. M.; Ioffe, I. N.; Cuniberti, G.; Dunsch, L.; Popov, A. A. *ACS Nano* **2011,** 5, 9939-9949.

27. Li, E. Y.; Marzari, N. *ACS Nano* **2011,** 5, 9726-9736.

28. Dai, J.; Zhao, Y.; Wu, X.; Zeng, X. C.; Yang, J. *J. Phys. Chem. C* **2013,** 117, 22156-22161.

29. Dresselhaus, M. S.; Dresselhaus, G.; Eklund, P. C., *Science of Fullerenes and Carbon Nanotubes*. Academic: San Diego, 1996.

30. Schumann, H. *Angew. Chem. Int. Ed.* **1984,** 23, 474-493.

31. Hitchcock, P. B.; Lappert, M. F.; Maron, L.; Protchenko, A. V. *Ang. Chem. Int. Ed.* **2008,** 47, 1488-1491.

32. Marks, T. J. *Organometallics* **2013,** 32, 1133-1136.

33. MacDonald, M. R.; Bates, J. E.; Ziller, J. W.; Furche, F.; Evans, W. J. *J. Am. Chem. Soc.* **2013,** 135, 9857-9868.

Chapter 3. Electronic and Optical Properties of Lanthanide SWNT Bis-Hexahapto Complexes

3.1 Introduction

The diversity of electronic structures available in organometallic complexes of the lanthanides has undergone a dramatic revision over the last 40 years. The organometallic complexes of the lanthanides were originally confined to the +3 oxidation state and the field was dominated by studies of the π-bonded tricyclopentadienyls [Ln(η^5-C_5H_5)$_3$], which are often associated in the solid state due to the their unsaturated coordination.[1] However, organometallic complexes of the +2 oxidation state followed and have been extended to all of the lanthanide elements[2] and zerovalent lanthanide organometallics have been characterized in which substituted benzene molecules function as the π-bonded ligand [Ln(η^6-^{t}Bu$_3$C$_6$H$_3$)$_2$].[3]

We have used this latter bonding motif to augment our use of the transition metal chemistry of the graphene surfaces of carbon nanomaterials,[4, 5] to enhance the conductivity of single-walled carbon nanotube (SWNT) networks by e-beam deposition of selected lanthanide atoms, Ln = La, Nd, Sm, Eu, Gd.[6] Prior to this work the deposition of chromium had led to the largest enhancement in the conductivity of the SWNT networks, exceeding the values obtained with M = Ti, V, Mn, Fe,[7] and M = Mo, W.[8] However, when we examined the lanthanide data we

found that there were two different behaviors: those which gave conductivity enhancements which were less than Cr and fairly typical of other transition metals examined to date (Ln = La, Nd, Gd), and those that exceeded the Cr values (Ln = Sm, Eu).[6] We were able to rationalize the conductivity data by reference to a model which is based on the accessibility of the $4f^m\ 5d^1\ 6s^2$ electronic configuration for the individual lanthanide atoms.[3, 9] In applying this model we suggested that the elements Sm and Eu were able to strongly enhance the conductivity of the SWNT films due to the ability of these metals to not only engage in bis-hexahapto-bonding [which is the characteristic feature of all of these (η^6-SWNT)M(η^6-SWNT) organometallic complexes], but to also transfer charge into the conduction band of the SWNTs due to the symmetry of the frontier molecular orbitals (FMOs) in the lanthanide complexes, and the fact that the partially filled metal 5d-orbitals involved in the interaction lie relatively high in energy in the case of Sm and Eu.[6]

Although the original work on the lanthanide complexes of benzene [Ln(η^6-^{t}Bu$_3$C$_6$H$_3$)$_2$], confirmed the formulation of these compounds as neutral, covalent, π-bonded molecules in which the metal was zerovalent,[3] the lanthanide compounds of C_{60} began with the idea that they would form salts[10] in analogy with the ionic alkali metal fullerides.[11, 12] Indeed the observation that some of these compounds (M = Yb, Sm) are superconductors strongly supports the idea that there are free electrons in these compounds which reside primarily on C_{60},[10, 13, 14] as do the physical properties of the Eu_xC_{60} compounds.[15] All of these authors assign the oxidation state of the lanthanide as +2 but the importance of covalent

character in these compounds is discussed at length.[14, 15] In this respect, the C_{60} compounds are rather different from the lanthanide complexes of benzene and SWNTs discussed above in that C_{60} is strongly curved and possesses five-membered rings (5-MRs); these features of the geometric and electronic structure contribute to the ability of the fullerenes to stabilize excess electron density.[16, 17] Although the fullerenes are incapable of forming stable π-complexes with transition metals requiring a hapticity greater than two, given the size and orbital extent of the lanthanides, they may be effective in facilitating η^5-coordination of the 5-MRs.[14, 18] Nevertheless, it is apparent that similar issues are relevant in the C_{60} and SWNT complexes of the lanthanides; that is, the question of covalent and ionic bonding, although the fullerides prepared to date only include M = Sm, Eu, and Yb which are known to readily form the +2 oxidation state.[3]

As noted above, we assigned a mixed [bis(hexahapto)] covalent, ionic structure to the compounds formed on interaction of the metals M = Sm, Eu with SWNT films on the basis of their strongly enhanced conductivities.[6] Given the importance of this question, we wanted to substantiate this suggestion with direct measurements of the charge density distributions in the (η^6-SWNT)M(η^6-SWNT) compounds, where M = Ln. Recently, we showed that both near-IR and Raman spectroscopy were able to provide such information in studies on SWNT films subjected to treatment with M = Au (physisorption), Li (chemisorption with ionic doping) and Cr (chemisorption with covalent hexahapto-bonding).[19] In the present paper we apply these techniques to SWNT films which have been subjected to

high vacuum e-beam lanthanide deposition as well as extending our studies to include additional lanthanides, M = Dy, Ho, Yb. We are able to confirm our previous assignments regarding the lanthanide charge density distributions and we show that this series of metals functions as both neutral bis(hexahapto) π-complexes [analogous to the $Ln(\eta^6\text{-}^tBu_3C_6H_3)_2$ compounds], but also as bis(hexahapto) π-complexes in which there is charge transfer to the conduction band of the SWNT backbone that further enhances the conductivity – in analogy with the M_xC_{60} compounds where M = Sm, Eu, Yb,[10, 13-15] In this chapter we will investigate the optical properties of each thin film to determine the type of bonding present in our samples and how this relates to the conductivity seen.

3.2 Experimental

The experiments made use of electric arc separated semiconducting (SC-) SWNTs obtained from NanoIntegris Inc. (IsoNanotubes, 99%), with average diameters of 1.2 - 1.7 nm and lengths of 300 nm to 2 μm.

3.2.1 Preparation of SWNTs films for Conductivity Measurements

The in situ conductivity measurements were performed with 8 nm thick SC-SWNT films prepared on alumina membranes via vacuum filtration. Film thickness was determined from SWNT density of 1.2 g/cm^3.[20] One milliliter of SWNT solution (0.01 mg/ml) was mixed with 50 mL of DI water, then vacuum filtered onto the

alumina membrane (Anodisc 47, 47 mm diameter, 0.02 μm) and was washed with a mixture of DI water and ethanol to remove remaining surfactant residues on the film. The alumina membranes were cut into 4 mm × 3 mm rectangles, positioned onto pre-patterned gold electrodes, and contacted with conductive silver paste. The films were annealed at 300^{o}C for 3 h at a pressure of 10^{-7} Torr to remove containments. The SC-SWNT films showed initial conductivities of σ = 2 S/cm.

3.2.2 Preparation of SWNTs films for Spectroscopy

The Near-IR (NIR) and Raman spectroscopic studies were performed on 4nm-thick SC-SWNT films prepared by vacuum filtration on nitrocellulose membranes (Millipore, 0.1 μm VCWP). These samples were made by first placing a small piece of SC-SWNT film on nitrocellulose membrane in contact with a thin borosilicate glass slide. Then the filter membrane was removed in a bath of acetone vapors over a period of one hour. The films were then annealed using the same conditions described above.

3.2.3 Metal Deposition

Li, Cr, Sm, Eu, Dy, Ho, Yb and Al deposition sources were obtained from Kurt Lesker. The *in-situ* conductivity measurements were carried out in a modified Temescal BJD 1800 E-Beam evaporator and used a Keithley 2700 to measure the two-point resistance of the samples. All films were exposed to the metal vapor at a deposition rate of 0.3-0.5 Angstroms per second at a chamber pressure of 2-5 x 10^{-6} torr. For the optical spectroscopy, 2.5 nm of the metal of interest was allowed

to deposit on half of the film. A homemade in-chamber shutter protected the other half from exposure to metal vapor and could be mechanically removed while keeping the chamber in high vacuum conditions. Once the shutter was removed, 50 nm of the covering metal (aluminum) was deposited. This gave each sample two distinct regions for characterization; a reference SC-SWNT film and a SC-SWNT film area which was exposed to the metal flux. The encapsulating Al layer allowed sample manipulation in the atmosphere without degradation of the metal-SWNT films.

3.2.4 Spectroscopy

Near infrared spectra were taken with a Jobin-Yvon iHR 320 spectrometer in combination with a Bruker Hyperion 1000 microscope and a MCT detector. Raman spectra were collected on a Nicolet Almega XS Raman spectrometer with 532 nm laser excitation and a laser power not exceeding 10%. To perform the measurements, we inverted the sample substrate, protected with an Al layer, and the spectra were taken through the glass slide. In the optical absorption measurements, the near-infrared radiation passed through the SWNT layer twice by reflection from the protective aluminum layer.

3.3 Results and Discussion

3.3.1 Conductivity measurements

The metal deposition experiments were performed on films of semiconducting (SC-) SWNTs (thickness, t = 8nm), which were mounted on substrates with gold contacts and transferred to a cryo-pumped Temescal BJD 1800 e-beam evaporator equipped with custom fittings to allow the measurement of the *in-situ* film resistance (Figure 3.1a);[7, 21] the initial resistance of the films was R = 1 MΩ (σ = 2 S/cm). In addition to the lanthanides, two other metals were included for comparison purposes: Cr, which forms a covalent hexahapto-bond to the SWNTs[7, 19, 22-27] and Li, which exhibits ionic doping of the SWNTs. The changes in the SWNT film conductivity on deposition of various metals are collected in Figure 3.1b and discussed in detail later in the paper. Briefly, charge transfer is exemplified by Li, which induces a linear enhancement of the SWNT film conductivity and produces a 100-fold increase in conductivity at t = 1 nm, whereas chromium shows an abrupt increase of conductivity which saturates beyond t = 0.2 nm. As noted previously,[6] in the initial stages of the deposition of the lanthanide metals (below 0.1 nm), there is a sharp increase in the SWNT conductivity which resembles the behavior of Cr. However, beyond this initial increase, the lanthanides exhibit two divergent behaviors in their effect on the SWNT conductivities: the enhancements produced by Dy, Ho and Gd are quite modest and show saturation, whereas Sm, Eu and Yb have a more pronounced effect.

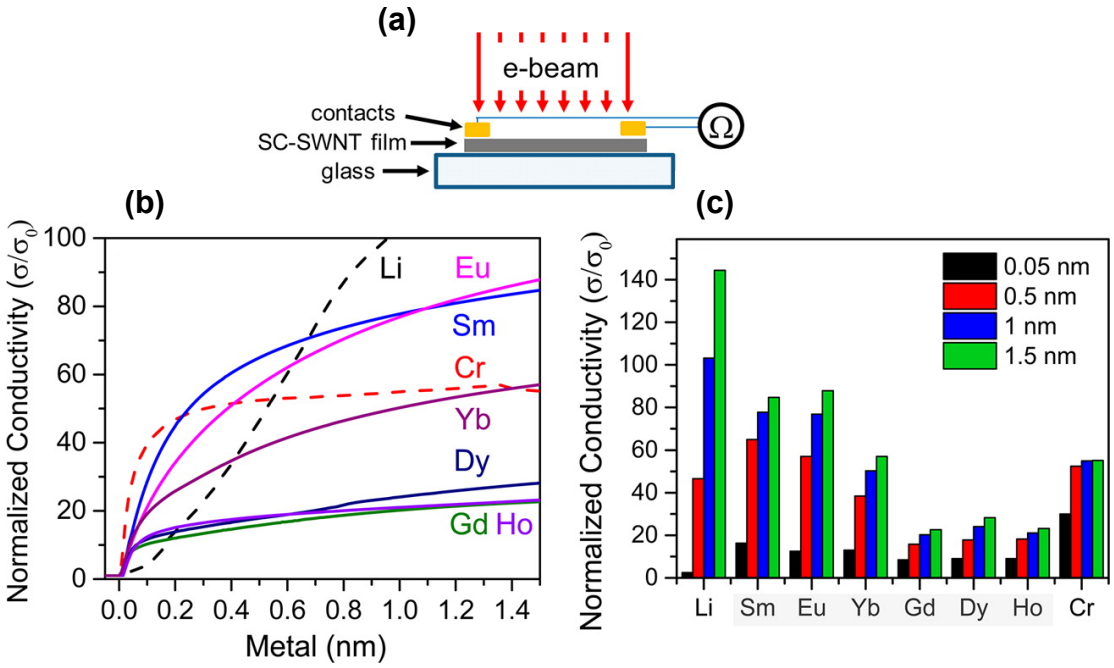

Figure 3.1 Effect of metal deposition on electrical conductivity of SC-SWNT films: (a) Schematic illustration of the experimental configuration of the in situ measurements of the film resistance during e-beam metal evaporation. (b) Change of SC-SWNT film conductivity as a function of deposited metal thickness; the values are normalized to the conductivity of pristine SC-SWNT film. (c) Normalized conductivities of SC-SWNT films with deposited metal of thicknesses 0.05, 0.5, 1 and 1.5 nm.

Figure 3.1c compares the conductivity increase due to the deposition of Li, Cr and the lanthanides. The data are normalized to the conductivity of the SC-SWNT films prior to deposition. It is apparent that at very low metal coverage (t = 0.05 nm) the effect of Li is very small, while Cr increases the film conductivity by more than 30 times and the lanthanides fall between these two extreme cases giving conductivity enhancements of ~10.

3.3.2 Spectroscopy

To spectroscopically characterize the effect of metal deposition on the SWNT samples it was necessary to remove the substrates from the e-beam apparatus and due to the sensitivity of the materials to the atmosphere, the

samples were coated with aluminum before exposure to the atmosphere. Thus, for the spectroscopic experiments, the SWNT films were mounted on thin borosilicate glass slides and 2.5 nm of the subject metal was deposited by e-beam evaporation (Li, Cr, Sm, Eu, Gd, Dy, Ho or Yb), followed by an aluminum protective layer (50 nm, e-beam). The optical measurements were performed in reflection mode through the thin borosilicate glass backside of the samples (Figure 3.2a).

Figure 3.2b displays a typical spectrum of the SC-SWNTs; the arc-discharge semiconducting SWNTs have an average diameter of 1.5 nm and their interband electronic transitions occur at ~0.6 eV (S_{11}) and ~1.1 eV (S_{22}). The intensities of these transitions are sensitive to the position of the Fermi level and electron donation shifts the Fermi level into the van Hove singularities, which

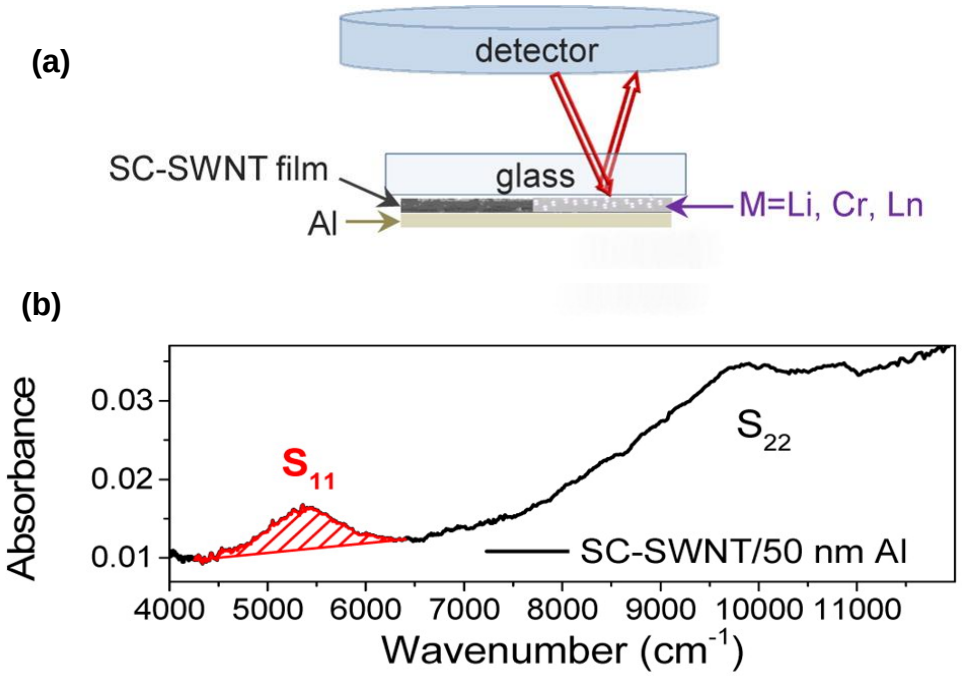

Figure 3.2 Absorption spectra of SWNT films as a function of metal deposition. (a) Schematics of sample configuration and measurement setup. (b) Spectrum of a SWNT sample covered with 50 nm aluminum layer. Dashed line illustrates the S_{11} region and the linear baseline correction.

suppresses the interband transitions due to Pauli blocking resulting in reduced peak intensities.[28-30] Thus, the intensities of the interband electronic transitions provide a sensitive indicator of the charge density on the SWNTs and in order to evaluate the electronic character of the interaction of the lanthanide metals with the SWNTs we studied the intensities of the S_{11} transitions of the SWNT films.

Figure 3.3 illustrates the baseline corrected spectra and in each experiment the spectrum of SC-SWNTs with deposited metal (2.5 nm) is compared with that of pristine SC-SWNTs collected from the same film. For comparison purposes the metal was deposited on one-half of the SWNT film, while the other half was protected from metal deposition by placement of a custom made shutter in the path of the metal flux. Following the deposition of the subject metal, the shutter was moved aside to allow the deposition of a 50 nm protective aluminum coating which covered the whole SWNT film, thereby allowing the simultaneous preparation of a sample with a metal-SWNT region and a pristine SWNT reference region in order to allow a direct comparison of the effect of the metal on the sample under study.

In agreement with our previous experiments, chromium deposition exerted little or no effect on the intensity of the S_{11} peak,[8, 19] and the same was true of the lanthanides Ln = Gd, Dy and Ho, thus suggesting that the enhancement in conductivity brought about by these metals is due almost entirely to metal hexahapto-bond formation.[6] Deposition of lithium completely suppressed the S_{11} transition, in accord with its strongly electron donating nature. Similarly, the optical

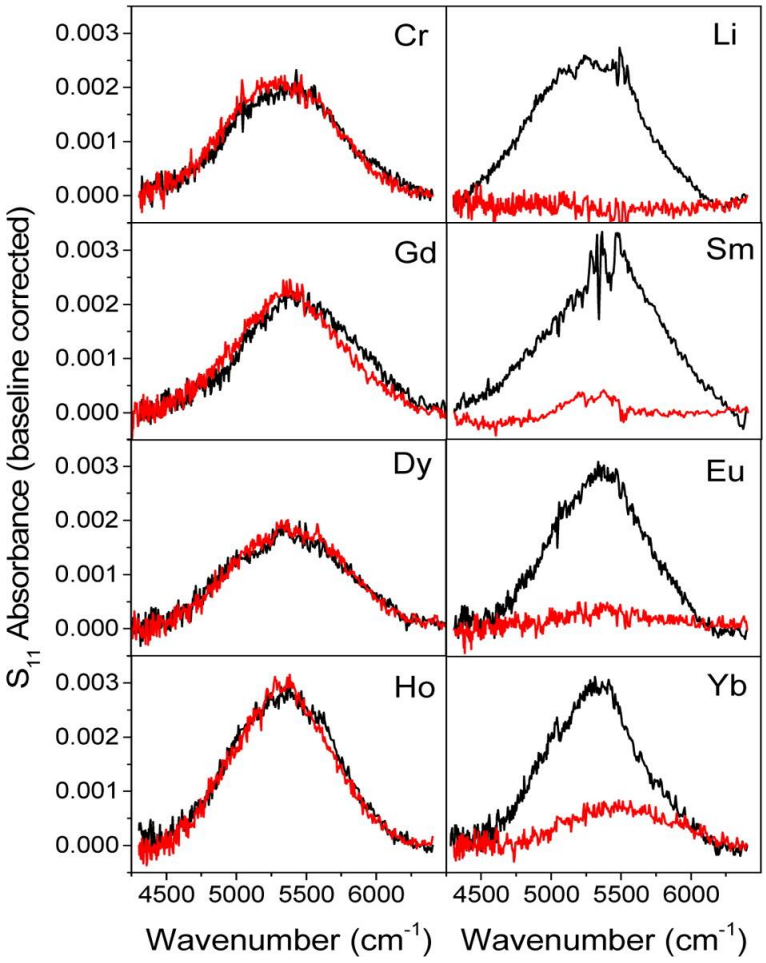

Figure 3.3 S11 interband transition of the nanotube films after baseline correction: reference (black, without metal) and sample (red, with deposited metal) (see text).

measurements showed that Sm and Eu almost completely suppress the S_{11} peak, while in the case of ytterbium there is still a detectable S_{11} peak suggesting a slightly weaker doping effect

3.3.3 Raman spectroscopy

The Raman spectrum of SWNTs is also sensitive to the charge density and Figure 3.4a gives a typical Raman spectrum of a SC-SWNT film; the spectrum displays four main features:[31] a G-peak - characteristic of all sp^2 hybridized carbon networks and associated with the Γ-point phonon mode; a small D-peak (disorder), associated with a K-point phonon mode which is activated by inelastic scattering of electrons on imperfections in the lattice such as defects, edges or grain boundaries; a radial-breathing mode (RBM) peak, related to the diameter of the nanotubes; and a 2D-peak, which is an overtone of the D-peak but its activation does not involve the presence of defects. In the presence of doping some of the associated phonon mode frequencies are renormalized due to electon-phonon coupling, resulting in a shift in the peak position.[32-34]. For the purposes of our experiments we focused on the effect of metal deposition on the 2D peak of the SWNT films. The 2D peak position in semiconducting SWNTs is downshifted by electron doping,[33] and this effect can be utilized to elucidate the extent of charge transfer between the active metal and the SWNTs.

The samples for the Raman experiments were prepared in the same way as for the absorption measurements (Figure 3.4a). Figure 3.4b shows a

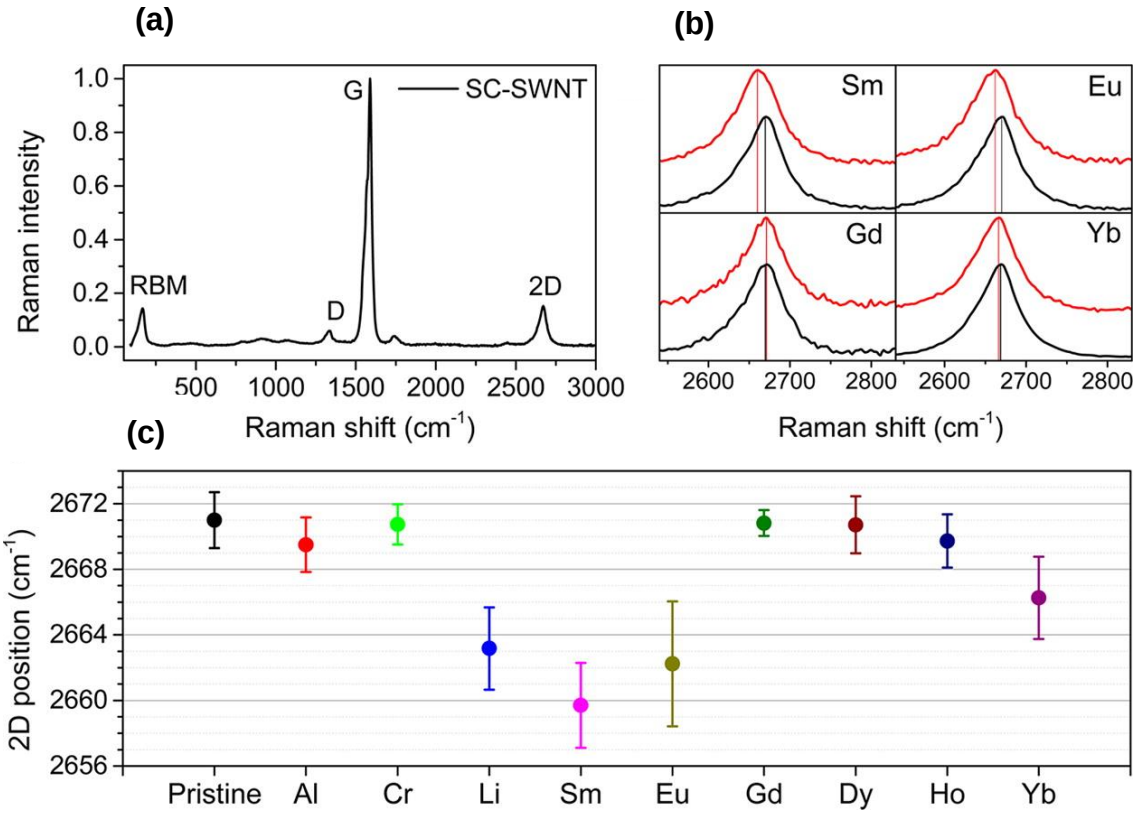

Figure 3.4 Raman spectroscopy of SWNT films as a function of metal deposition. (a) Raman spectrum of a SC-SWNT film. The four most prominent features are labeled: RBM, radial breathing mode, D, disorder peak, G, graphitic peak, 2D peak, peak overtone of the D peak. (b) 2D region of the Raman spectra of selected samples of SWNT films with deposited metal (M = Sm, Eu, Gd, and Yb) (red) and reference spectra (black, pristine SCSWNT) (see text). (c) Mean and standard deviation of 2D peak positions of the samples.

comparison of the spectra of selected samples; black curves represent the reference SC-SWNT region, while red curves show the Raman spectrum of the region with deposited active metal. Multiple spots were measured on each sample and the mean values are compared in Figure 3.4c. Li, Sm and Eu induce a large downshift corresponding to significant electron donation from the metal to the nanotube, while Yb only moderately shifts the 2D peak position of the SC-SWNTs. Cr, Al, Gd, Dy, and Ho show little or no effect on the peak position, indicating the absence of ionic character in their interaction with the SWNTs.

The standard model of bis-hexahapto-lanthanide complexation requires the participation of the $4f^m\ 5d^1\ 6s^2$ lanthanide electronic configuration,[3, 9, 35] and this mode of bonding operates with a 15 electron valence shell electronic structure. According to this model the stability of the bis-hexahapto-lanthanide complexes depends on the accessibility of the $5d^1\ 6s^2$ electronic structure and we have previously shown that such an analysis accounts for the variations in the conductivity enhancements measured for the series, Ln = La, Nd, Sm, Eu, Gd.[6] In this analysis, we suggested that the additional enhancement in the conductivities induced by Eu and Sm relative to the other lanthanides (La, Nd, Gd) was due to the ability of Eu and Sm to transfer electron density to the SWNT conduction band via the bis-hexahapto-bonds at the SWNT junctions.[6] Thus it was of interest to explore the relationship of the Raman 2D peak shift due to electron density donation to the SWNTs (Figure 3.5a), with the promotion energy necessary to achieve the $4f^m\ 5d^1\ 6s^2$ lanthanide electronic configuration and it may be seen in

Figure 3.5a that the Raman data suggest that Eu, Sm and Yb are able to transfer electrons to the SWNT conduction band.

Although all of the metals enhance the SWNT film conductivities, there are distinct differences in the character of the conductivity response (Figure 3.1): the transition metals and lanthanides are characterized by an abrupt change in conductivity at low coverage ($t \leq 0.2$ nm), whereas simple doping (Li), shows a more gradual, continuous increase in the film conductivity which we have attributed to the transfer of electrons to the SWNT conduction band.[4, 7] Furthermore, in our studies of the effect of Au, Li and Cr on the percolation threshold of very thin SWNT films it was apparent that the ability of Cr to form bis-hexahapto bonds and thereby bridge SWNT junctions was most apparent at low metal coverage due to the very small number of sites with the geometry necessary for this reaction.[19] To capture the distinction between these two modes of metal-SWNT interactions we introduce the differential conductivity enhancement ($\Delta\sigma$), which in the present context we define as $\Delta\sigma = [\sigma_{(t = 1.0\ nm,\ metal)} - \sigma_{(t = 0.2\ nm,\ metal)}]/\sigma_o$ (where σ_o is the conductivity of the pristine SWNT film), with the goal of defining an index of covalent and ionic character in metal-SWNT bonding. Based on the previous discussion this parameter should be directly related to the promotion energy necessary to achieve the $4f^m\ 5d^1\ 6s^2$ lanthanide electronic configuration (as shown in Figure 3.5b), because this latter quantity determines the relative placement of the lanthanide d-orbitals and the SC-SWNT conduction band.[6]

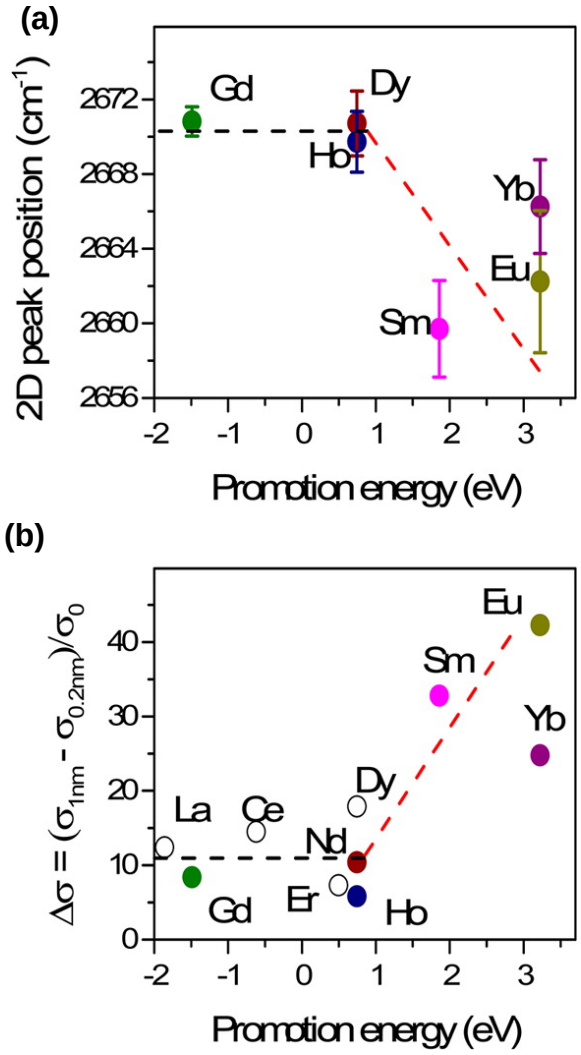

Figure 3.5 Relationship of the lanthanide promotion energies (see text), to the Raman shifts and conductivities of the SWNT networks after lanthanide deposition. (a) Promotion energy as a function of the Raman 2D peak position. (b) Promotion energy as a function of the differential conductivity enhancement, $\Delta\sigma = (\sigma_{1nm} - \sigma_{0.2nm})/\sigma_0$. Dashed lines are guides to the eye.

3.4 Conclusion

The differential conductivity ($\Delta\sigma$), which provides a measure of the conductivity enhancement as a function of coverage, reflects the contribution of ionic character in the (η^6-SWNT)Ln(η^6-SWNT) hexa-hapto bonds. Low values of $\Delta\sigma$ imply purely covalent bonding (La, Nd, Gd, Dy, Ho), whereas an increase in $\Delta\sigma$ is associated with the involvement of charge transfer to the SWNT conduction band in addition to hexa-hapto bond formation (Eu, Sm, Yb). As expected, $\Delta\sigma$ is related to the promotion energy necessary to achieve the $4f^m\ 5d^1\ 6s^2$ lanthanide electronic configuration (Figure 3.5b), because this latter quantity dictates the energetics of the charge transfer process.[6] Thus, we conclude that all of the lanthanides exhibit the initial abrupt increase in conductivity at low coverage which is characteristic of the transition metals, but only Eu, Sm, Yb show the continually increasing conductivity characteristic of strong electron donors (Figures 3.1 and 3.5b, large values of $\Delta\sigma$), and this supports our contention that these latter metals provide the first examples of mixed covalent–ionic bis-hexahapto bonds [(η^6-SWNT)M(η^6-SWNT), where M = Sm, Eu, Yb].[6]

The ability to modify and interconnect the electronic structures of graphitic surfaces by single atom covalent and ionic bonding (atomtronics), [5] suggests the application of this approach in catalysis, high mobility transistor, spintronic and memory devices.[23, 36, 37] Furthermore, there is the promise of new ferromagnetic and superconducting materials based on the organometallic single layer graphene

and graphene sandwich compounds and their relationship to the graphite and C_{60} intercalation compounds.[4, 5, 10, 12-15, 22, 36, 38]

References

1. Schumann, H. *Angew. Chem. Int. Ed.* **1984,** 23, 474-493.

2. MacDonald, M. R.; Bates, J. E.; Ziller, J. W.; Furche, F.; Evans, W. J. *J. Am. Chem. Soc.* **2013,** 135, 9857-9868.

3. Cloke, F. G. N. *Chem. Soc. Rev.* **1993**, 17-24.

4. Bekyarova, E.; Sarkar, S.; Wang, F.; Itkis, M. E.; Kalinina, I.; Tian, X.; Haddon, R. C. *Acc. Chem. Res.* **2013,** 46, 65-76.

5. Sarkar, S.; Moser, M. L.; Tian, X.; Zhang, X. J.; Al-Hadeethi, Y. F.; Haddon, R. C. *Chem. Mater.* **2014,** 26, 184-195.

6. Moser, M. L.; Tian, X.; Pekker, A.; Sarkar, S.; Bekyarova, E.; Itkis, M. E.; Haddon, R. C. *Dalton Trans.* **2014,** 43, 7379-7382.

7. Wang, F.; Itkis, M. E.; Bekyarova, E.; Tian, X.; Sarkar, S.; Pekker, A.; Kalinina, I.; Moser, M.; Haddon, R. C. *Appl. Phys. Lett.* **2012,** 100, 223111.

8. Kalinina, I.; Bekyarova, E.; Sarkar, S.; Wang, F.; Itkis, M. E.; Tian, X.; Niyogi, S.; Jha, N.; Haddon, R. C. *Macromol. Chem. Phys.* **2012,** 213, 1001-1019.

9. Anderson, D. M.; Cloke, F. G. N.; Cox, P. A.; Edelstein, N.; Green, J. C.; Tanya Pang ; Sameh, A. A.; Shalimoff, G. *J. Chem. Soc., Chem. Commun.* **1989**, 53-55.

10. Ozdas, E.; Kortan, A. R.; Kopylov, N.; Ramirez, A. P.; Siegrist, T.; Rabe, K. M.; Bair, H. E.; Schuppler, S.; Citrin, P. H. *Nature* **1995,** 375, 126-129.

11. Haddon, R. C.; Hebard, A. F.; Rosseinsky, M. J.; Murphy, D. W.; Duclos, S. J.; Lyons, K. B.; Miller, B.; Rosamilia, J. M.; Fleming, R. M.; Kortan, A. R.; Glarum, S. H.; Makhija, A. V.; Muller, A. J.; Eick, R. H.; Zahurak, S. M.; Tycko, R.; Dabbagh, G.; Thiel, F. A. *Nature* **1991,** 350, 320-322.

12. Haddon, R. C. *Acc. Chem. Res.* **1992,** 25, 127-133.

13. Chen, X. H.; Roth, G. *Phys Rev B* **1995,** 52, 15534-15536.

14. Citrin, P. H.; Ozdas, E.; Schuppler, S.; Kortan, A. R.; Lyons, K. B. *Phys. Rev. B.* **1997,** 56, 5213-5227.

15. Ginwalla, A. S.; Balch, A. L.; Kauzlarich, S. M.; Irons, S. H.; Klavins, P.; Shelton, R. N. *Chem. Mater.* **1997,** 9, 278-284.

16. Haddon, R. C.; Brus, L. E.; Raghavachari, K. *Chem. Phys. Lett.* **1986,** 125, 459-464.

17. Haddon, R. C. *Philos. Trans. R. Soc., A* **1993,** 343, 53-62.

18. Haddon, R. C. *J. Comput. Chem.* **1998,** 19, 139-143.

19. Tian, X.; Moser, M. L.; Pekker, A.; Sarkar, S.; Ramirez, J.; Bekyarova, E.; Itkis, M. E.; Haddon, R. C. *Nano Lett.* **2014,** 14, 3930-3937.

20. Wang, F.; Itkis, M. E.; Haddon, R. C. *Nano Lett.* **2010,** 10, 937-942.

21. Wang, F.; Itkis, M. E.; Bekyarova, E.; Sarkar, S.; Tian, X.; Haddon, R. C. *J. Phys. Org. Chem.* **2012,** 25, 607-610.

22. Tian, X.; Sarkar, S.; Moser, M. L.; Wang, F.; Pekker, A.; Bekyarova, E.; Itkis, M. E.; Haddon, R. C. *Mater. Lett.* **2012,** 80, 171-174.

23. Avdoshenko, S. M.; Ioffe, I. N.; Cuniberti, G.; Dunsch, L.; Popov, A. A. *ACS Nano* **2011,** 5, 9939-9949.

24. Li, E. Y.; Marzari, N. *ACS Nano* **2011,** 5, 9726-9736.

25. Dai, J.; Zhao, Y.; Wu, X.; Zeng, X. C.; Yang, J. *J. Phys. Chem. C* **2013,** 117, 22156-22161.

26. Ketolainen, T.; Havu, V.; Puska, M. J. *J. Chem. Phys.* **2015,** 142, 054705.

27. Gloriozov, I. P.; Marchal, R.; Saillard, J.-Y.; Oprunenko, Y. F. *Eur. J. Inorg. Chem.* **2015,** 2015, 250-257.

28. Itkis, M. E.; Niyogi, S.; Meng, M.; Hamon, M.; Hu, H.; Haddon, R. C. *Nano Lett.* **2002,** 2, 155-159.

29. Pichler, T.; Liu, X.; Knupfer, M.; Fink, J. *New J. Phys.* **2003,** 5, 156.

30. Wu, Z.; Chen, Z.; Du, X.; Logan, J. M.; Sippel, J.; Nikolou, M.; Kamaras, K.; Reynolds, J. R.; Tanner, D. B.; Hebard, A. F.; Rinzler, A. G. *Science* **2004,** 305, 1273-1276.

31. Dresselhaus, M. S.; Saito, R.; Hofmann, M.; Dresselhaus, G.; Jorio, A. *Adv. Phys.* **2011,** 60, 413-550.

32. Tsang, J. C.; FreitagM; PerebeinosV; LiuJ; AvourisPh. *Nat. Nanotechnol.* **2007,** 2, 725-730.

33. Das, A.; Sood, A. K. *Phys Rev B* **2009,** 79, 235429.

34. Corio, P.; Santos, P. S.; Brar, V. W.; Samsonidze, G. G.; Chou, S. G.; Dresselhaus, M. S. *Chem. Phys. Lett.* **2003,** 370, 675-682.

35. Di Bella, S.; Lanza, G.; Fragala, I. L.; Marks, T. J. *Organometallics* **1996,** 15, 3985-3989.

36. Sarkar, S.; Zhang, H.; Huang, J.-W.; Wang, F.; Bekyarova, E.; Lau, C. N.; Haddon, R. C. *Adv. Mater.* **2013,** 25, 1131-1136.

37. Liu, X.; Wang, C.-Z.; Hupalo, M.; Lin, H.-Q.; Ho, K.-M.; Tringides, M. C. *Crystals* **2013,** 3, 79-111.

38. Sarkar, S.; Niyogi, S.; Bekyarova, E.; Haddon, R. C. *Chem. Sci.* **2011,** 2, 1326-1333.

Chapter 4. Fast Electrochromic Device Based on Single-Walled Carbon Nanotube Thin Films

4.1 Introduction

The ability to control optical properties of materials by application of electric field finds a wide range of applications in electro-optical modulators and optical interconnects for high speed optoelectronics and optical communication. These applications utilize Pockel's, Kerr, Franz-Keldysh and quantum-confined Stark effects in non-linear crystals, conventional semiconductors and heterostructures. Recent progress in this area has allowed the expansion of their bandwidth of operation to the GHz range.[1] Another class of electrochromic devices makes use of an electrochemical cell in which the active electrochromic layer changes its optical transmittance or reflectance in the desired spectral range upon modulation of its charge state which in turn is compensated by its proximity to the ions of electrolyte.[2-6] Typical response times of electrochemical cell based electrochromic devices are in the range of tens to hundreds of seconds. Despite the slow response such systems have recently attracted significant attention in connection with the development of smart windows for climate control and energy conservation in the buildings and for use in rear view mirrors in vehicles, [2-6] and some progress over last decade has been made in improving response time of these devices utilizing nanostructured materials.[5] Among electrolyte based systems the fastest response

times of 5 to 30 ms were reported for nanostructured poly(3,4-ethylenedioxythiophene) (PEDOT) based electrochromic devices.[7, 8]

Recently, thin films of carbon based nanostructured materials such as single-walled carbon nanotubes (SWNTs) and graphene have shown the ability to modulate optical transmittance under the application of a gate voltage in solid state field effect transistor (FET) or electro-chemical cell configurations.[9-18] Solid state gating allows fast response, but shows a low modulation depth which is typically less than 1% of the absorption signal.[10, 11] In our recent work, the amplitude of the photoresponse was enhanced to ~7% through utilization of large diameter separated semiconducting (SC-) SWNTs with the bandwidth extending beyond 100 kHz.[14] Alternatively, the utilization of electrolytes in an electrochemical optical cell configuration has achieved a high depth of electro-optical modulation in SWNT and graphene thin layers, but a slow response time which is typically in the tens to hundreds of seconds range.[9, 12, 16, 18, 19]

Ionic liquids have recently emerged as a highly efficient and environmentally friendly alternative to traditional electrolytes with mobile anions and cations of small sizes that are capable of accumulating extremely high charge carrier density at the electrolyte - solid state material interface in which the solid state material becomes a part of electric double layer capacitor with a sub-nanometer dielectric gap.[20] By utilizing metallic (MT-) SWNTs in combination with an ionic liquid it was possible to modulate the optical transparency of the electrochemical cell in the

visible spectral range and to realize various color changes based on different MT-SWNTs diameters with the response time reduced to 1 s.[21] Further reduction in the response time would expand the functionality of electrochromic systems and the field of their application.

Here we report the fabrication of a SWNT thin film based electro-optical modulator in which the active electrochromic layer is made of a film of sorted SC-SWNTs and the counter-electrode is composed of a film of MT-SWNTs with an ionic liquid utilized as electrolyte. We show that optimization of such electro-optical (EO) cells allowed a 100-fold increase in the operation speed with a significant amplitude of modulation of infrared transmittance maintained up to frequencies between 100 to 1000 Hz.

4.2 Experimental

4.2.1 Device Fabrication

SWNT thin film based electro-optical modulator was composed of two semitransparent conducting layers supported by glass substrates and sealed together by an adhesive frame (Frame-SealTM, Bio-Rad Laboratories) of thickness 250 μm with inner space filled with ionic liquid [N,N-diethyl-N-(2-methoxyethyl)-N-methylammonium bis-(trifluoromethylsulphonyl)-imide, DEME-TFSI] purchased from IoLiTec Inc. as presented in schematic in Figure 4.1a.

Electro-optically active layer was formed of semitransparent film of large diameter (~1.55 ±0.1 nm) 99% separated SC-SWNTs purchased from Nanointegris Inc. Counter-electrode was prepared using thin film of 99% separated MT-SWNTs or single layer CVD graphene. SC-SWNT and MT-SWNT films were prepared by vacuum filtration and transferred on glass substrates to bridge 2 mm gap between pre-deposited Pd(10nm)/Pt(100nm) electrodes; the Pd/Pt combination of metals shows better electrochemical stability than Cr/Au electrodes which showed some degradation under voltage cycling. The pairs of addressing Pd/Pt lines on the opposite sides of the cell were oriented at 90^{o} to define 2mm X 2mm electro-optical window. Modifications of spectral characteristics of the electrochromic cell were tested utilizing a Cary 5000 UV-Vis-NIR spectrophotometer.

4.2.2 AC and DC Measurements

Amplitude and dynamic of electro-optical response were studied using a lock-in amplifier technique utilizing a pair of infrared LED and photodiode operating in the vicinity of wavelength 1800 nm closely matching the maximum of the S_{11} absorption band of SC-SWNTs. Current to the infrared LED (Model 1800P, Thorlabs) was provided by an ultra-low distortion function generator (Model DS360, Stanford Research Systems). For AC measurements the signal from the InGaAs photodiode (Model FD10D, Thorlabs) was captured with a lock-in amplifier (Model SR830, Stanford Research Systems). An oscilloscope (model TDS 1001C-

EDU, Tektronix) was connected to the ac amplifier output of the lock-in amplifier to capture the waveforms of the response during the experiment. For DC measurements the photodiode signal was routed to a data acquisition system that captured the waveforms of the response via ExceLINX (Keithley). The sample voltage was modulated by a synthesized function generator (Model DS345, Stanford Research Systems). The LED and photodiode were mounted utilizing separate XY Lens Positioners (Newport) and were placed on an optical bread board facing each other. In between the two, an electrochromic cell holder was placed on the board. After preliminary alignment of all three components was established by reaching maximum signal, all components were bolted down and precision alignment was achieved with the X and Y knobs on both positioners. An electrical control box was made to house the reverse bias current source and the load resistors circuits for the LED and for the photodiode, respectively. The reverse bias of 0.2 V was supplied by a programmable electrometer (Model 617, Keithey) for all AC and DC experiments. The control box was also used to route all of the above stated electronic circuits through all of the measurements and was used to switch “on” and “off” the proper circuits when needed. Response time was evaluated from the frequency dependence and oscilloscope traces of electrotransmittance response assuming, for simplification, exponential decay process with single exponential time constant.

4.2.3 Spectroscopic Measurements

Transmission/Absorption spectra of SWNT thin film based electro-optical cells were measured as a function of gate voltage utilizing Cary 5000 UV-Vis-NIR spectrophotometer (Agilent). DC gate voltage across the electro-optical cell in the range +3V to -3V was supplied by Keithley model 617 source-meter.

4.3 Results and Discussion

4.3.1 Modulation of Absorption Spectra of SC-SWNT Thin Film Electrochromic Cell under Applied Voltage

A schematic of the electro-optical cell is presented in Figure 4.1 with the active electrochromic layer of SC-SWNTs of variable thicknesses and optical densities and counter-electrode layer of 16 nm thick highly transparent film of MT-SWNTs. Both films were composed of large diameter SWNTs (D_{av} = 1.55 nm), supported on glass substrates and sealed together with an adhesive frame filled inside with ionic liquid.

The SWNT films were electrically addressed by two orthogonal pairs of Pd/Pt electrodes forming a 2 x 2 mm^2 electro-optical window. Figure 4.2a shows modification of absorption of the EO cell made utilizing 58 nm thick SC-SWNT film under application of voltage across the EO cell when scanned between -3 V and +3 V (the range of electrochemical stability of the ionic liquid). At zero voltage the

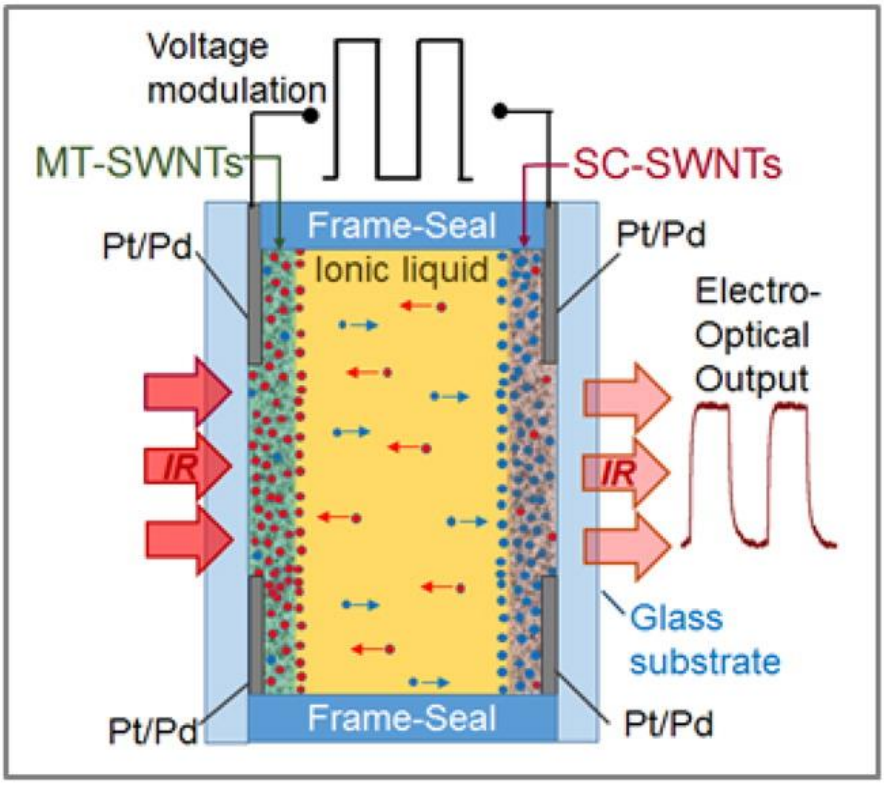

Figure 4.1 Schematics of SWNT thin film based electrochromic cell with electro-optically active SC-SWNT electrode and MT-SWNT counter-electrode.

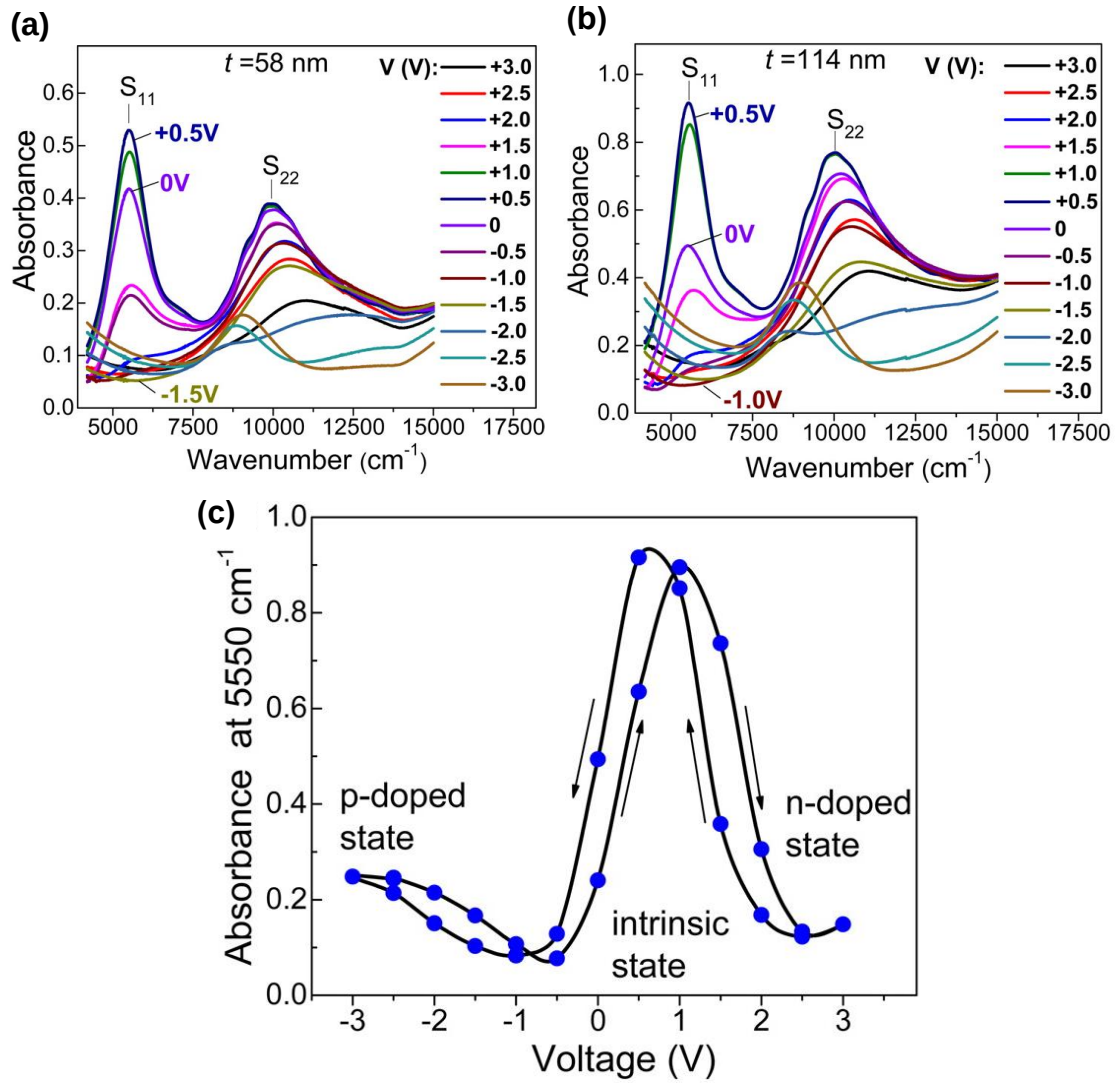

Figure 4.2 Spectral modulation of SC-SWNT thin films of thickness: (a) 58 nm, and (b) 114 nm, as a function of voltage. (c) Absorbance at wavenumber 5550 cm^{-1} (center of S_{11} band) as a function of voltage.

S_{11} absorption band is suppressed due to environmental p-doping of SC-SWNTs[22] and it requires application of voltage of + 0.5V to the MT-SWNT electrode to achieve the intrinsic state of the SC-SWNTs which give rise to the maximum S_{11} band absorption *A* of 0.53 at wavenumber 5550 cm^{-1}. Application of a voltage of +3.0 V leads to a strongly n-doped state with populated conduction bands, S_{c1} and S_{c2}, while the application of -3.0 V results in strong p-doping with depleted valence bands, S_{v1} and S_{v2}, both resulting in bleaching of S_{11} and S_{22} interband transitions. The minimum absorption at wavenumber 5550 cm^{-1} of 0.05 was achieved at a voltage of -1.5 V, so sweeping the voltage between +0.5 V and -1.5 V leads to the maximum change of absorption ΔA of ~0.48.

Figure 4.2b shows a similar spectral modulation in a device with thickness of SC-SWNT film increased to 114 nm. As expected, a stronger change of absorption ΔA ~0.83 was achieved in the case of the thicker SC-SWNT film on sweeping the voltage from +0.5 V (*A*=0.91, intrinsic state) to -1.0 V (*A*=0.08, p-doped bleached state). The voltage sweep of the SC-SWNT film shows hysteretic behavior of the absorbance at the center of the S_{11} band at 5550 cm^{-1} (Fig.4.2c), with a hysteretic offset of about 0.5 V which cannot be completely eliminated by increasing the dwell time. This hysteretic behavior is typical for electrolyte controlled charge accumulation systems and corresponds to the different potentials required for the ions to enter or exit the electroactive layers during the voltage cycles.[20]

4.3.2 Dependence of Electrotransmittance on SC-SWNT Film Thickness

The quasi-static properties of the SC-SWNT thin film based electro-optical modulator and related figures of merit are presented in Figure 4.3 as a function of SC-SWNT film thickness. SC-SWNT film thicknesses from 12 to 114 nm with identical counter-electrodes made of 16 nm thick films of MT-SWNTs. The gate voltage was cycled between the bleached "on" state (maximum transmittance T_{MAX}, p-doped SWNT state) and opaque "off" state (minimum transmittance T_{MIN}, intrinsic SWNT state) in square-wave form at low frequency (0.1 Hz). For the 12 nm thick SC-SWNT film the transmittance changes between ~81% and 64% for the "on" and "off" states, respectively, resulting in ΔT~17%. With increasing SC-SWNT film thickness the modulation of the transmittance became more and more pronounced reaching ΔT~64% for the 114 nm thick film.

Figure 4.3b summarizes the overall behavior of the transmittance in "on" and "off" states and the transmittance modulation ΔT as a function of thickness. Transmittance in the "on" (bleached) states decreases from 81 to 68% with increasing film thickness from 12 to 114 nm with an overall rate of decrease of ~ 0.13%/nm. The 18% loss of transmittance at the limit of zero thickness of the SC-SWNT films is mainly due to reflections at the four interfaces of the two glass substrates of refractive index n_G=1.5 with a reflection of ~4% at each interface, totaling ~16%. This loss could be reduced by utilizing antireflective coatings and different substrate materials.

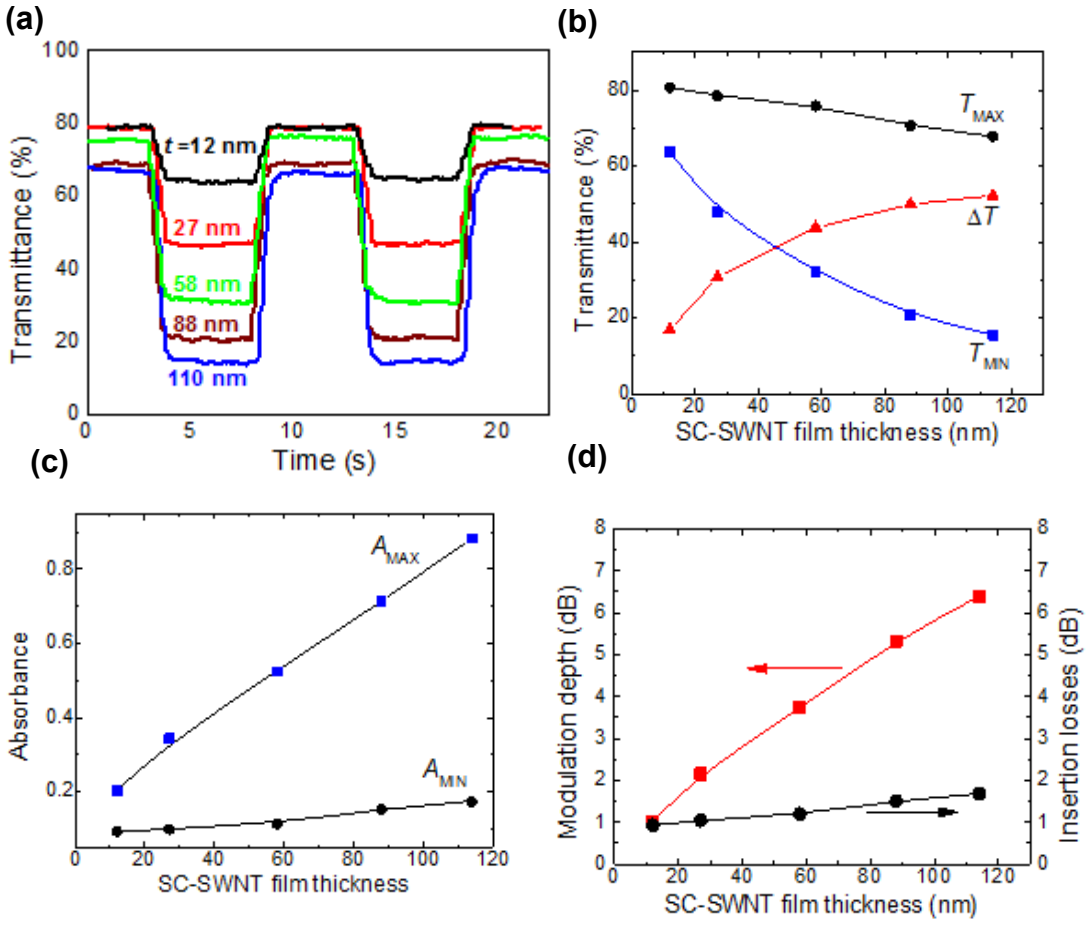

Figure 4.3 (a) Electrotransmittance response of SC-SWNT thin films on square-wave pulses of the gate voltage at a quasi-static modulation frequency of 0.1 Hz, as a function of thickness. (b) Dependence of the maximum and minimum transmittance values and transmittance modulation ΔT on the thickness of the SC-SWNT film. (c) Dependence of maximum and minimum absorbance A on thickness of SC-SWNT film. (d) Dependence of modulation depth and insertion losses on the thickness of the SC-SWNT film.

The MT-SWNT counter-electrode and the ionic liquid together are responsible for only about 2% of the transmittance loss. The transmittance in the "off" (dark) state is suppressed much more dramatically with increasing SC-SWNT film thickness, although the modulation of the transmittance ΔT shows sublinear behavior with saturation at high thicknesses. Figure 4.3c presents data from Figures 4.3a and 4.3b in terms of absorbances A_{MAX} and A_{MIN} in "off" and "on" states, respectively, as a function of SC-SWNT film thickness. As expected for the case of homogeneous media, absorbances in both states increase approximately linear with increasing SC-SWNT film thickness. The linear increase of absorbance and the absorbance modulation leads to the saturation behavior observed for ΔT in Figure 4.3b due to the non-linear relationship between these quantities, $T=10^{-A}$.

On the basis of the above results, the SWNT thin film EO modulator can be characterized in terms of two common performance metrics: the modulation depth and the insertion losses as a function of SC-SWNT film thickness. The modulation depth (or extinction ratio) expressed in decibels as $10\log(T_{ON}/T_{OFF})$[1] is presented in Figure 4.3d: it increases from 1 to 6.4 dB as the film thickness is increased from 12 to 114 nm and can be further enhanced by increasing the thickness of SC-SWNT films. The insertion loss expressed as $-10\log(T_{ON}/100)$ [1] increases slowly with increasing SC-SWNT film thickness from 0.9 to 1.7 dB and is comprised of a thickness dependent component related to the minimum absorption of the SC-SWNT film in the fully bleached state and a thickness independent insertion loss

of ~ 0.9 dB mostly due to reflections at the glass substrate interfaces, as discussed above.

4.3.3 Frequency Dependence of Electrotransmittance Response

In the following part of the paper we report our studies of the dynamic properties of the SWNT thin film based electrochromic device. Figure 4.4a shows oscilloscope traces of the electrotransmittance response of the electro-optical modulator utilizing a SC-SWNT film of thickness 58 nm as the active layer. With increasing frequency of the square-wave gate voltage modulation the shape of the response changes from near square-wave at 1 Hz to triangular at 1000 Hz with decreasing amplitude. The ionic liquid controlled SC-SWNT thin film modulator is capable of approaching saturated “on” and “off” states at cycling frequencies of 100 Hz and maintains a significant modulation depth up to frequencies of 1000 Hz in a striking contrast to the electrolyte based electrochromic devices which typically exhibit response times up to hundreds of seconds.[4, 6] Figure 4.4b shows the waveforms of the electrotransmittance response of the EO cells with different thicknesses of SC-SWNT film at a fixed frequency of 50 Hz voltage modulation. At film thicknesses below 58 nm response times in the millisecond range are achieved while with increasing thickness a triangular photoresponse waveform with a response time above 10 ms is observed.

Figure 4.4c presents the frequency dependences of electrotransmittance response for electrochromic devices with different SC-SWNT film thicknesses.

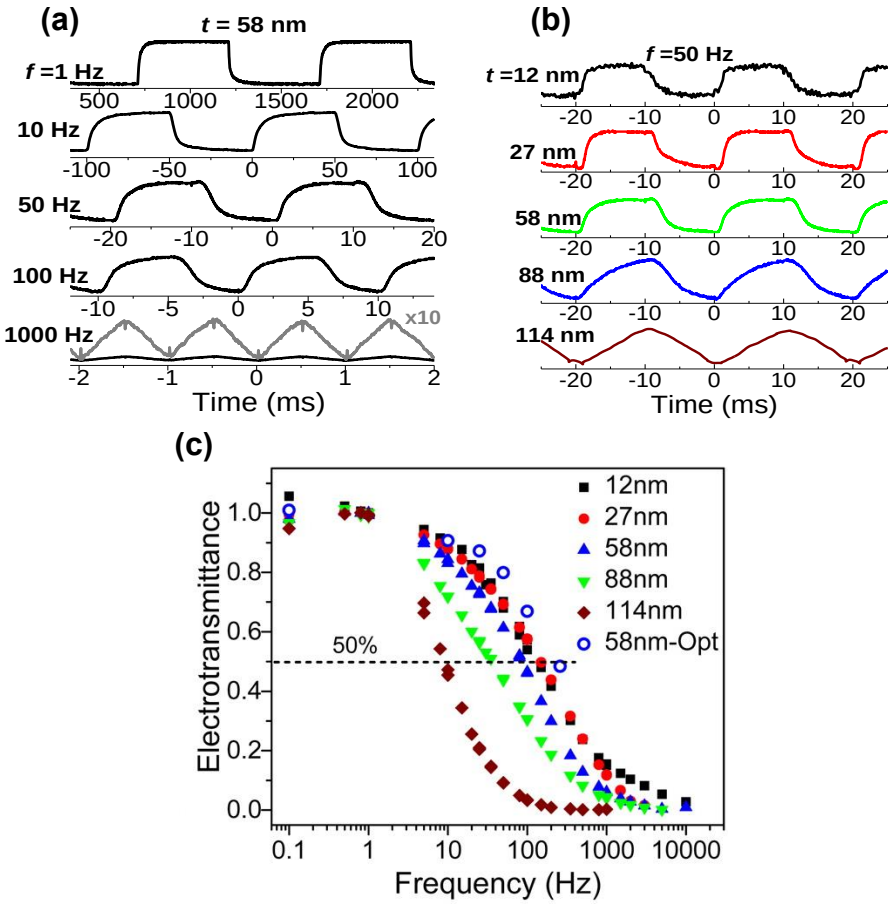

Figure 4.4 (a) Waveforms of electrotransmittance response for different modulation frequencies for a device utilizing a SC-SWNT film of thickness 58 nm; (b) Waveforms of electrotransmittance response as a function of thickness of SC-SWNT film at fixed modulation frequency of 50 Hz. (c) Frequency dependencies of electrotransmittance response for devices with different SC-SWNT film thicknesses. Open circles (labeled 58nm-Opt) correspond to data obtained for 58 nm SC-SWNT film with amplitude of voltage modulation optimized at each frequency.

The corresponding performance metric, the Modulation Bandwidth (MBW), defined in literature by the frequency *f*(50%) at which the modulation is reduced to 50% of its maximum value[1] is presented in Figure 4.5a (blue columns) as a function of SC-SWNT film thickness. The highest MBW value of ~140 Hz was obtained for thinner films of 12 and 27 nm. For 58 nm film the MBW value was 87 Hz and decreased below 10 Hz for the thickest (114 nm) SC-SWNT film. Corresponding response times τ were evaluated utilizing *f*(50%) values, $\tau = (\sqrt{3})/(2\pi f(50\%))$, assuming, for simplification, exponential approach to equilibrium $(1-\exp(-t/\tau))$ with a single time constant. As a result, response times of 1.9 and 3.2 ms were obtained for 27 nm and 58 nm thick films, respectively, as presented in Figure 4.5c. Alternatively, under the same exponential decay simplification, the response time can be evaluated from the oscilloscope traces as time required to reach (1-1/*e*) or ~ 63% of the saturation value (Figure 4.5a,b). The obtained values are in the range of the *f*(50%) based determination, but show a decrease with increasing frequency of square-wave excitation (Figure 4.5c). Such a decrease corresponds to the exclusion of slower processes, involving less accessible ion destinations within the SWNT network, from the overall ionic liquid polarization, when the period of square-wave electromodulation shortens. Another, accepted in the literature, definition of the response time corresponds to the time required to reach 90% of equilibrium transmittance value[7, 8] and, typically, gives 2-3 times longer response times as illustrated in Figure 4.5c.

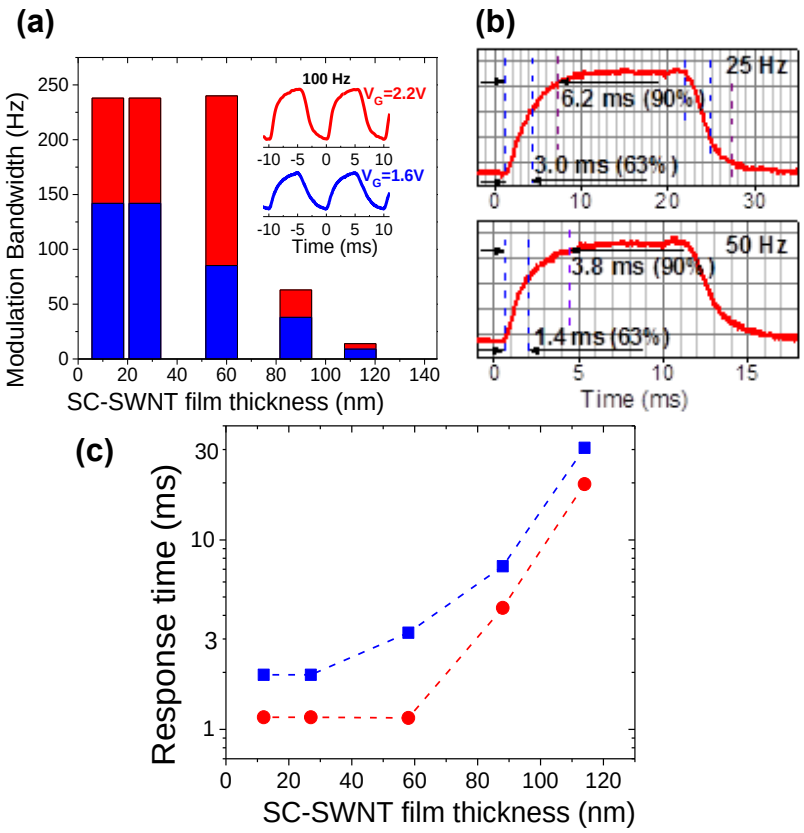

Figure 4.5 (a) Modulation Bandwidth of electrotransmittance response as a function of SC-SWNT film thickness for the modulation amplitude optimized at frequency 1 Hz (blue columns) and at each frequency (diagonal pattern). Inset shows oscilloscope traces of electro-optical response at different amplitudes of voltage modulation V_G. (b) Determination of response time for 58 nm SC-SWNT film device using 63% and 90% rise criteria for 25 Hz and 50 Hz pulses for V_G optimized at each frequency; (c) Response times of electromodulation as function of SC-SWNT film thickness for V_G optimized at a frequency of 1 Hz (blue squares) and at each frequency (red circles).

In SWNT based electrochromic devices, complex dynamics of the electrotransmittance response is defined by the electric field induced diffusion of ions across the thickness of the porous SWNT network involving equilibrium sites of different accessibility, thus resulting in a wide distribution of response times, from fraction of a millisecond to seconds, as exhibited by a fast onset and more sluggish than exponential saturation of the response (Figure 4.4, 4.5). Thus, we use as a primary the *f*(50%) based definition of the response time,[1] as it provides a reasonable account of statistical weights of individual contributions across the whole range of ions redistribution processes, with other definitions also presented for comparison.

The experiments described above were conducted at a fixed amplitude of voltage modulation optimized at 1 Hz. The electrotransmittance response can be enhanced by increasing the amplitude of voltage modulation at high frequencies within the range of stability of the ionic liquid (±3.0V). As shown in Figure 4.4c and figure 4.5a, such voltage optimization leads to enhanced electro-optical modulation at high frequencies, increasing MBW to 240 Hz for the SC-SWNT film thicknesses 12-58 nm, and accordingly, faster response time $\tau \leq 2$ ms (Figure 4.5c, *f*(50%) based definition) due to faster diffusion of the ions across the active SC-SWNT electrochromic layer enforced by the higher electric field.

The results presented in Figure 4.5 indicate that the response time of the SWNT thin film EO modulator is affected by the diffusion of the ions within the

thickness of the SWNT film (10-100 nm) as the charge distribution comes to equilibrium in the electric double layer capacitor. As the SC-SWNT film thickness (t) increases from t = 27 nm to t = 58 nm (Δt ~ 30 nm) the response time increases from 1.9 ms to 3.2 ms ($\Delta\tau$ ~ 1.3 ms), which allows an estimate of the diffusion speed (v_d) in the 58 nm thick film, of $v_d = \Delta t/\Delta\tau \sim 2.4*10^{-3}$ cm/s. On further increase of the thickness of SC-SWNT layer to t = 114 nm the diffusion slows down significantly (τ ~ 30 ms), corresponding to effective values of $v_d \sim 3*10^{-4}$ cm/s, and we adopt a film thickness of 30-60 nm in order to provide an optimum balance of the static and dynamic properties of the SWNT thin film based EO modulator. For comparison, the reported ion drift speed in conventional electrolytes is in the range of 10^{-5} -10^{-2} cm/s.[23, 24]

4.3.4 Effect of Inter-Electrode Spacing on the Dynamic of Electro-Optical Response

To evaluate the effect of the inter-electrode spacing on the dynamics of the electro-optical response, we compared the waveforms and frequency dependencies of the electrotransmittance response for two devices with standard (250 μm) and increased (1 mm) inter-electrode spacing and the results are presented in Figure 4.6a,b. The observed decrease of the cutoff frequencies (Figure 4.6b, f(50%)) from 87 Hz to 57 Hz corresponds to an increase of the response time from 3.2 ms to 4.9 ms (3.1 ms to 4.7 ms from the oscilloscope traces, Figure, 4a), as the separation d is changed from 0.25 to 1 mm, thereby

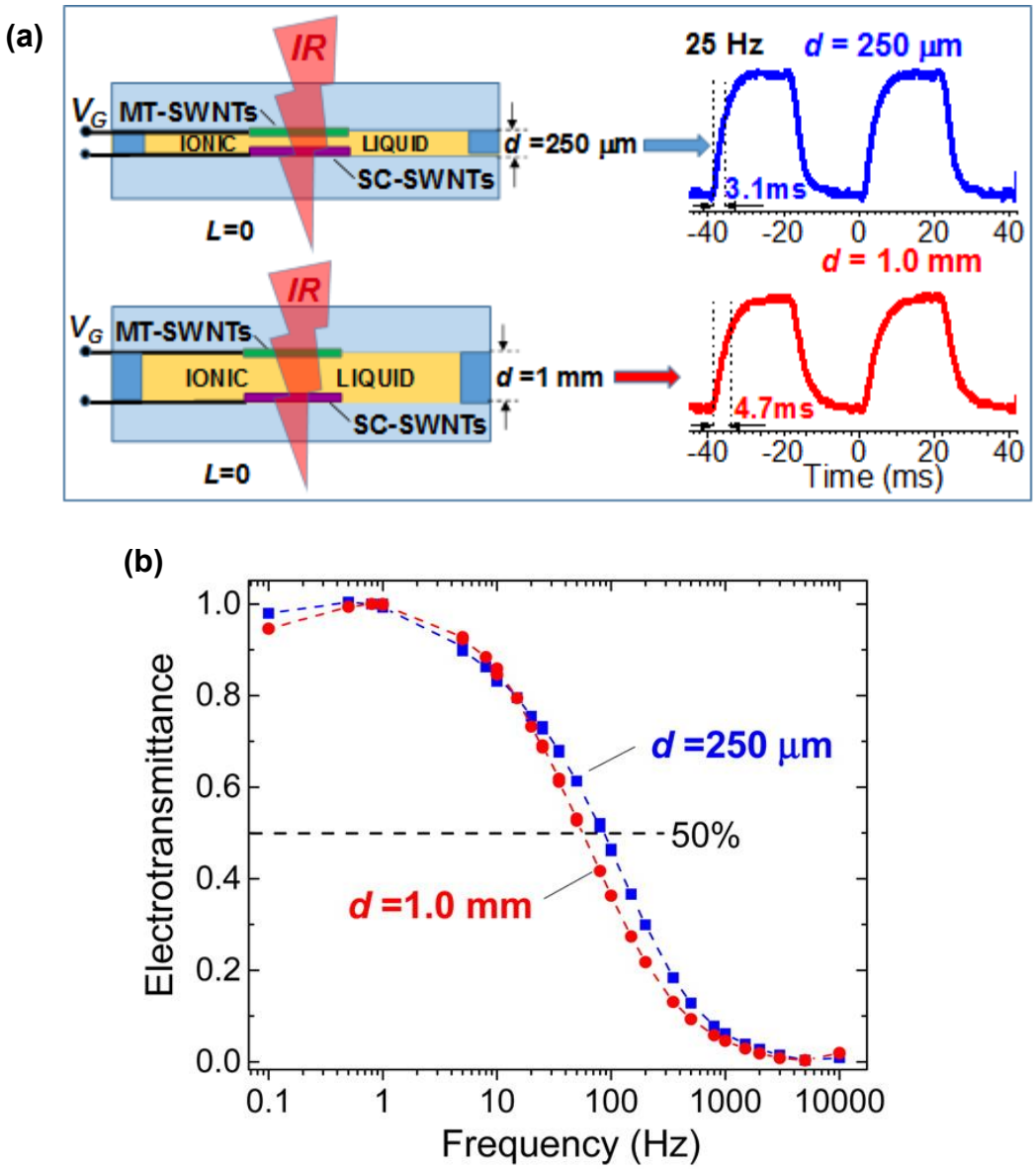

Figure 4.6 Effect of increasing inter-electrode spacing *d* from 250 μm to 1 mm on (a) electrotransmittance waveform (response time) at modulation frequency 100 Hz and (b) frequency dependence of electrotransmittance.

providing an estimate of the rate of response time increase: $\Delta\tau/\Delta d$ = ~0.23 ms/100 μm. The observed difference in response time is quite small and an additional experiment was conducted with a larger electrode separation of 4.5 mm which utilized a lateral shift of the electrodes (Figure 4.7a) instead of the usual vertical configuration that was impractical for large distances. The thickness of SC-SWNT films in this set of experiments was 27 nm.

The lateral shift of 4.5 mm resulted in a much stronger change of the cutoff frequencies (response times) which decreased (increased) from 133 Hz (2.1 ms) to 16 Hz (17.2 ms) (Figure 4.7a,b), leading to a rate of response time increase: $\Delta\tau/\Delta d$ = ~0.35 ms/100 μm comparable to the previous estimate. The increase of the response time with increasing inter-electrode separation originates from the decrease of the electric field driving the ion diffusion processes. An inter-electrode separation of 250 μm is adequate for the current device configuration, but it is feasible to decrease it below 100 μm in conjunction with further optimization of the porosity, bundle size and thicknesses of both SC- and MT-SWNT films in order to further expand the bandwidth of operations of SWNT based electrochromic devices.

4.3.5 Dependence of Electrotransmittance Response on Counter Electrode Material

In addition to the use of a MT-SWNT film as the counter-electrode, several alternative materials were evaluated. The most commonly used transparent

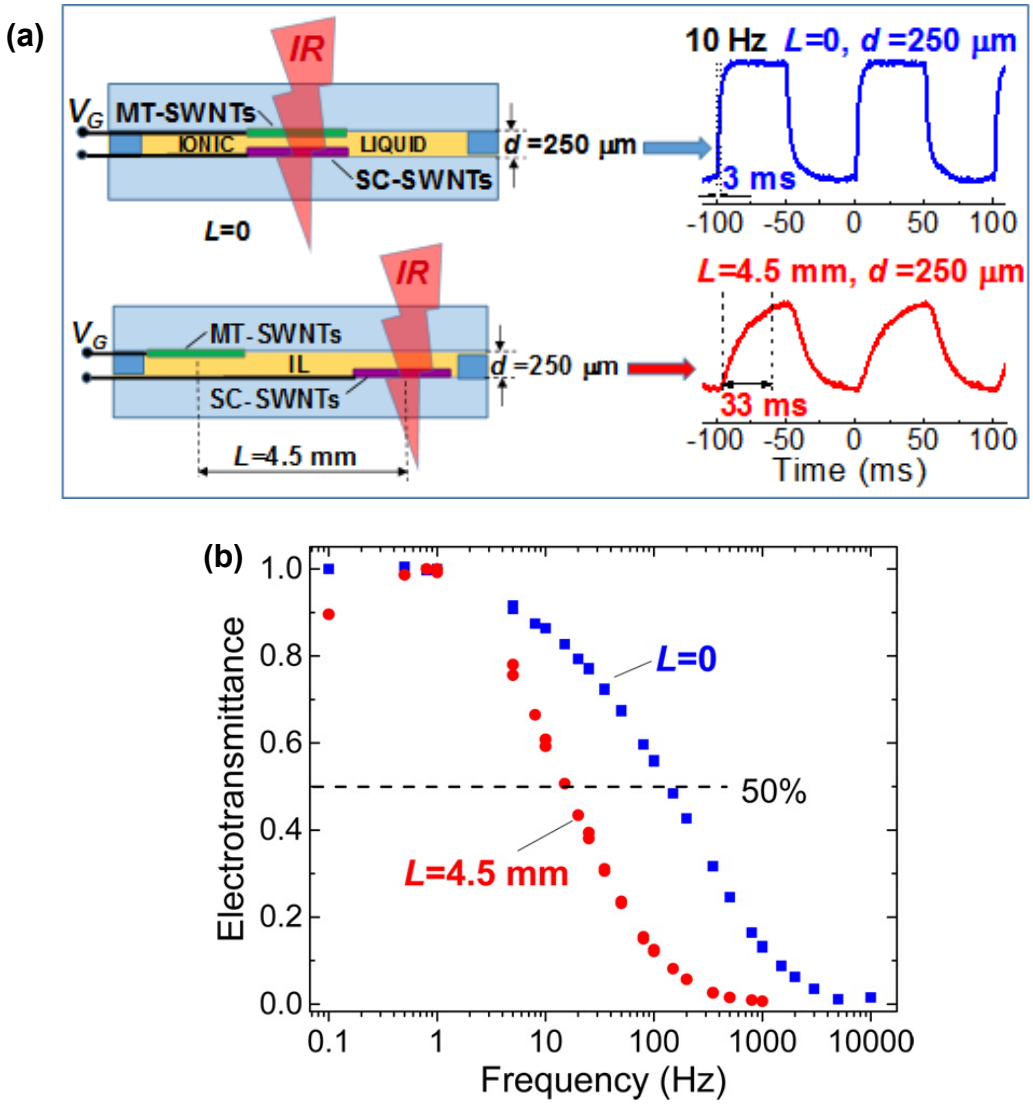

Figure 4.7 Effect of lateral shift L=4.5 mm between SC-SWNT electrode and MT-SWNT counter-electrode on (a) electrotransmittance waveform (response time) at modulation frequency 10 Hz and (b) frequency dependence of the electrotransmittance.

conductor, indium tin oxide, is not transparent in the near- or mid-infrared spectral ranges and is therefore not a candidate for this application. Single layer graphene (SLG) has recently emerged as a new option in this class of materials because of its high transparency (98%) and high electrical conductivity[25, 26] and thus we tested SLG as replacement for the MT-SWNT film. A comparison of MT-SWNT and graphene counter-electrodes is presented in Figure 4.8(a,b) in terms of the response waveform at modulation frequency 25 Hz and its frequency dependence.

The utilization of a graphene counter-electrode resulted in much slower response than in case of MT-SWNT film: Modulation Bandwidth *f*(50%) decreased by a factor of four from 87 Hz to 21 Hz (Fig.4.8b) and corresponding response time increased from 3 to 13 ms. The amplitude of low frequency response at 1 Hz was not significantly affected by the graphene substitution, but with increasing frequency the advantage of MT-SWNT counter-electrode became more and more evident as shown in Figure 4.8a,b. In addition, a device without graphene (or SWNT) counter-electrode in which the gate potential was provided by two remaining Pt/Pd addressing lines separated by 2 mm opening showed slow response time and frequency dependence similar to the case of the graphene counter-electrode. The advantage of 16 nm MT-SWNT film over graphene in this application can be ascribed to the high porosity of MT-SWNT film and a high surface area which is, theoretically, 25 times higher than that of a single sheet of graphene. This allows the construction of an efficient electric double layer

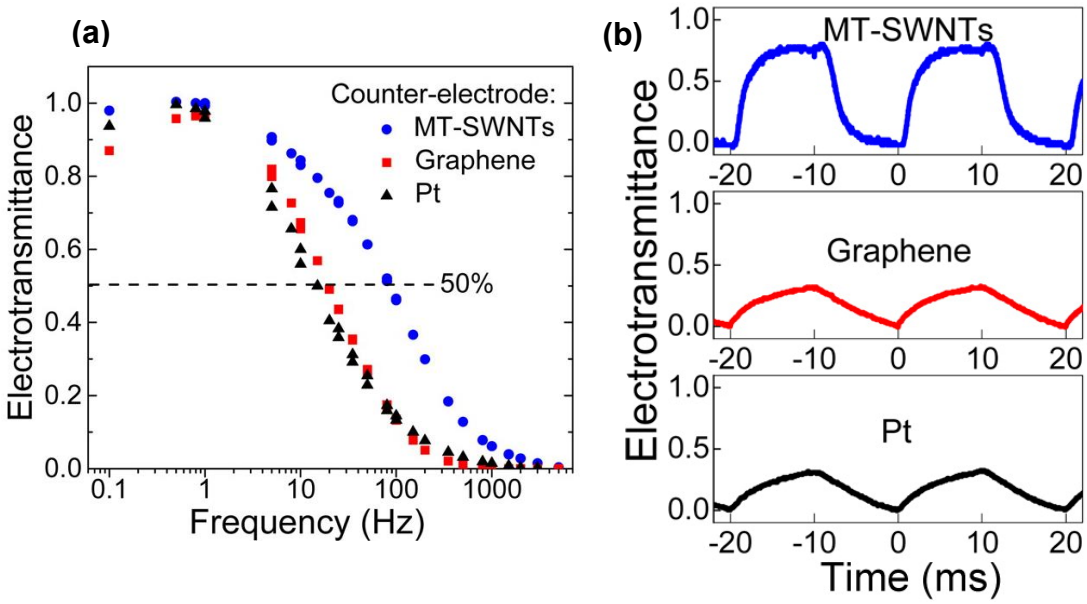

Figure 4.8 Comparison of (a) waveform of electrotransmittance pulses at modulation frequency 25 Hz and (b) frequency dependence of electrotransmittance for different counter-electrode materials: MT-SWNTs, graphene and Pt.

capacitor which is capable of extremely high accumulated carrier density that can rapidly compensate the charge at the SC-SWNT counter-electrode.

Aging of the SC-SWNT thin film EO modulator with MT-SWNT counter-electrode was studied under continuous cycling at a modulation frequency 1 Hz and results are presented in Figure 4.9. Only 2% decrease of the amplitude of the EO response after 25,000 cycles with no significant changes in the response shape (response time) was observed thus indicating excellent long-term stability of the SWNT thin film-ionic liquid electro-optical modulator.

4.3.6 Dual Electro-Optical Devices Based on SC-SWNT Electrodes

Most electrochromic devices utilize one electro-optically active electrode while the counter-electrode plays a passive role for the application of electrical potential as in the case of the MT-SWNT film above. Alternatively, it is possible to improve the efficiency by constructing dual electrochromic devices in which both electrodes are electro-optically active. [8, 13] A schematic of a SWNT based dual EO device in which both electrodes are formed by electro-optically active SC-SWNT films of thickness 58 nm is presented in Figure 4.10a. The SC-SWNT films were annealed in vacuum at 350^{o}C before the device assembly to restore the intrinsic state of SC-SWNTs. In addition, graphene underlayers were added to the SC-SWNT films to establish a uniform potential across the electrochromic area and to supply current to the device when the electrical conductivity of SC-SWNT film is suppressed in the intrinsic (insulating) state. Figure 4.10b shows the modification

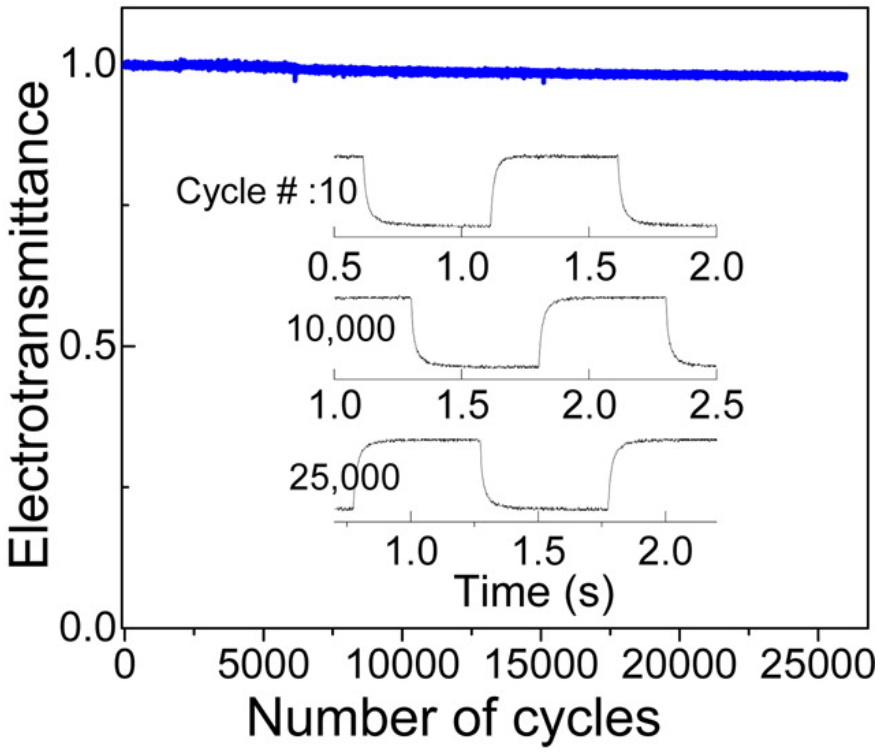

Figure 4.9 Long-term stability of the electrotransmittance response over 25,000 modulation cycles of a device with SWNT electrodes. Inset shows conservation of the amplitude and shape of electrotransmittance pulses from the beginning to the middle (10,000 cycles), and end (25,000 cycles) of long term stability study.

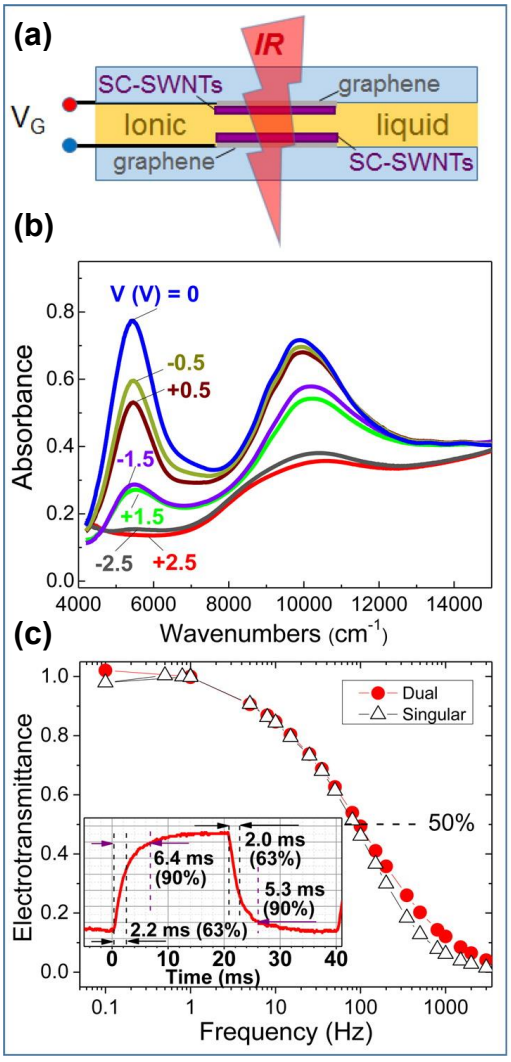

Figure 4.10 Dual electro-optical cell in which both electrodes are made of electro-optically active SC-SWNT thin film. (a) Schematic of the dual device; (b) Absorbance spectra as a function of voltage; (c) Frequency dependence of electrotransmittance under unipolar square-wave voltage modulation. Inset shows oscilloscope traces of electrotransmittance response to 25 Hz square-wave voltage modulation.

of the static absorbance spectra of the dual electrochromic device under an applied gate voltage and Figure 4.11b shows the absorbance value at the center of absorption band at 5550 cm^{-1} as a function of the applied voltage. The maximum absorbance in the S_{11} band is achieved at zero voltage and the minimum absorbance at +2.5 V and -2.5 V. The application of the gate voltage results in a shift of chemical potential into the conductance band in one SC-SWNT film (n-doping) and into the valence band of the opposing SC-SWNT film (p-doping) as illustrated in density of states (DOS) insets in Figure 4.11b; both shifts result in bleaching of the S_{11} transition and a highly transparent state, while at zero voltage both electrodes are at the intrinsic state with maximum S_{11} absorption. An advantage of the dual active electrode device is the higher modulation depth of 6.7 dB in comparison with the value of 3.7 dB for a single active layer device of the same SC-SWNT film thickness. It is feasible to exceed 10 dB modulation depth by a moderate increase of the thickness of SC-SWNT films.

The dual electrochromic device also maintains the fast response time τ=2.8 ms (2.2 ms), as obtained from the frequency dependence (oscilloscope traces) of electrotransmittance (Figure 4.10c, *f*(50%)=99Hz). This response is slightly faster than for single active layer device, because the higher operating voltage required for the annealed SC-SWNT films forces faster diffusion of the ions.

The dual device configuration provides additional functionality by electro-optically doubling the frequency of the initial voltage modulation. In order to

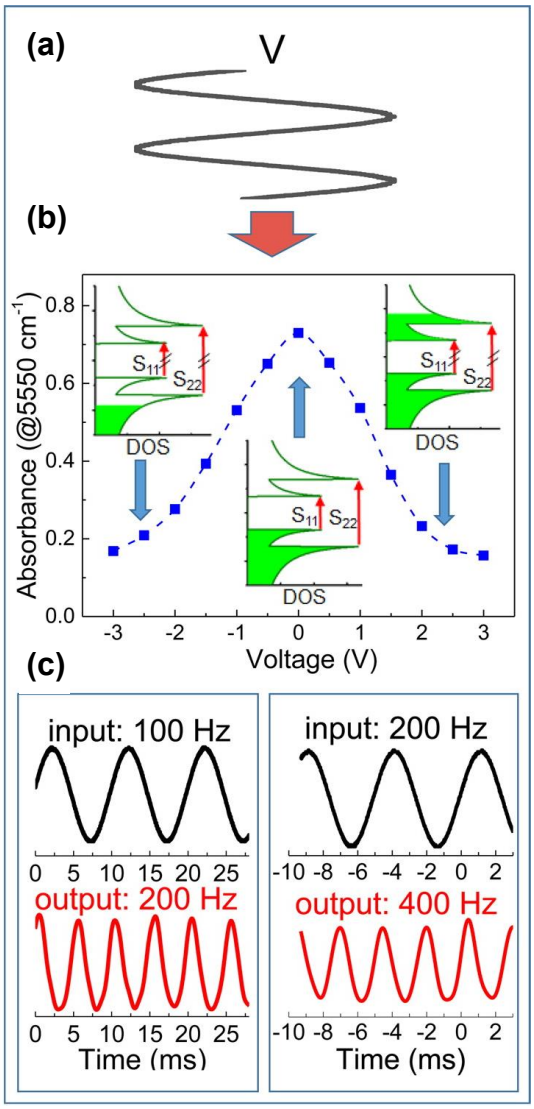

Figure 4.11 (a) Symmetric sine-wave voltage modulation combined with (b) symmetric voltage dependence of absorbance of dual electro-optical cell leads to (f) doubling of the frequency of the initial voltage modulation. Insets in (c) show electronic density of states corresponding to p-doped (negative voltage), intrinsic (zero voltage) and n-doped state (positive voltage) of SC-SWNT thin film.

demonstrate this function a symmetric sine modulation waveform is applied to the dual device (Figure 4.11a) resulting in the passage through the bleached (highly doped) state at both positive and negative voltages and also passage though the opaque (intrinsic) state twice per cycle as shown in Figure 4.11b. As a result, the dual electrochromic device converts, for example, 100 Hz or 200 Hz voltage oscillation into 200 or 400 Hz EO response, respectively, as shown in Figure 4.11c.

SWNT thin film based electrochromic devices can be compared to commercially available Fast Optical Shutters (FOS) from LC-Tec (Sweden)[27] whose performance is based on electric field driven reorientation of the birefringent liquid crystal (LC) molecules. The LC based shutters show comparable switching times in the 1 – 30 ms range (longer opening times, typically, 15-30 ms), but have an advantage of higher contrast up to 1000:1 over the current SWNT system. Both systems are vibration-free with no moving parts and have a small footprint, but the SWNT based devices allow lower operating voltage 1-3 V as compared to 5 – 24 V for the LC-Tec systems. The current study involves the evaluation of the electro-optical modulation in the vicinity of 1800 nm wavelength compared to FOS devices operating in the visible and near-infrared (1100 nm) spectral range. The operational wavelength can be modified by utilization of SWNTs of different diameters (different bandgaps) in order to cover the visible and near-infrared spectral ranges and expanded into the 8-14 μm long-wave infrared region by utilizing the low energy absorption tail,[16, 28] well beyond the current limitations of the LC-Tec based systems. In order to create useful technology, the contrast

(modulation depth) of the SWNT based system should be enhanced, for example, by increasing the SWNT film thickness or a multi-layer design. The contract enhancement should be performed while maintaining or decreasing response times by tuning the SWNT thin film pore structure and exploring ionic liquids with different ion sizes and high diffusivities.

4.4 Conclusion

In summary, an ionic liquid controlled infrared electro-optical modulator composed of a SC-SWNT electro-optically active electrode and transparent conducting counter-electrode was explored. By optimizing the thickness of the SC-SWNT thin film and the type of counter-electrode material a modulation depth of 3.7 dB and fast operations with millisecond range response time were achieved. Utilization of a MT-SWNT thin film transparent counter-electrode resulted in faster operations and stronger modulation than a graphene counter-electrode because of the much higher surface area of the SWNT film. A dual electro-optical modulator in which both electrodes were made of electro-optically active SC-SWNT films showed an enhanced modulation depth of 6.7 dB, millisecond range response time and the capability to electro-optically double the frequency of the initial voltage modulation. The efficient electro-optical modulation is a result of the high porosity and high surface area of SWNT thin films which allow fast penetration of the ions and the formation of a 3-dimensional electric double layer capacitor involving the

full thickness of the SWNT layer. The development of fast electrochromic systems provides an opportunity to expand the field of thin film SWNT optoelectronics into smart window applications, infrared modulators and shutters, and infrared imaging systems.

References

1. Reed, G. T.; Mashanovich, G.; Gardes, F. Y.; Thomson, D. J. *Nature Photon.* **2010,** 4, 518-526.

2. Baetens, R.; Jelle, B. P.; Gustavsen, A. *Sol. Energ. Mat. Sol. Cells* **2010,** 94, 87-105.

3. Llordes, A.; Garcia, G.; Gazquez, J.; Milliron, D. J. *Nature* **2013,** 500, 323-326.

4. Granqvist, C. G. *Thin Solid Films* **2014,** 564, 1-38.

5. Runnerstrom, E. B.; Llordes, A.; Lounis, S. D.; Milliron, D. J. *Chem. Commun.* **2014,** 50, 10555-10572.

6. Mortimer, R. J.; Rosseinsky, D. R.; Monk, P. M. S. e., *Electrochromic Materials and Devices*. Wiley-VCN Verlag GmbH & Co. KGaA: Veinheim, Germany, 2013.

7. Cho, S. I.; Kwon, W. J.; Choi, S.-J.; Kim, P.; Park, S.-A.; Kim, J.; Son, S. J.; Xiao, R.; Kim, S.-H.; Lee, S. B. *Adv. Mater.* **2005,** 17, 171-175.

8. Jain, V.; Yochum, H. M.; Montazami, R.; Heflin, J. R. *Appl. Phys. Lett.* **2008,** 92, 033304.

9. Wu, Z.; Chen, Z.; Du, X.; Logan, J. M.; Sippel, J.; Nikolou, M.; Kamaras, K.; Reynolds, J. R.; Tanner, D. B.; Hebard, A. F.; Rinzler, A. G. *Science* **2004,** 305, 1273-1276.

10. Takenobu, T.; Murayama, Y.; Shiraishi, M.; Iwasa, Y. *Jpn. J. Appl. Phys.* **2006,** 45, L1190-L1192.

11. Takenobu, T.; Murayama, Y.; Iwasa, Y. *Appl. Phys. Lett.* **2006,** 89, 263510.

12. Kavan, L.; Dunsch, L. *ChemPhysChem* **2007,** 8, 974-998.

13. Nikolou, M.; Dyer, A. L.; Steckler, T. T.; Donoghue, E. P.; Wu, Z.; Heston, N. C.; Rinzler, A. G.; Tanner, D. B.; Reynolds, J. R. *Chem. Mater.* **2009,** 21, 5539-5547.

14. Wang, F.; Itkis, M. E.; Haddon, R. C. *Nano Lett.* **2010,** 10, 937-942.

15. Liu, M.; Yin, X.; Ulin-Avila, E.; Geng, B.; Zentgraf, T.; Ju, L.; Wang, F.; Zhang, X. A. *Nature* **2011,** 474, 64-67.

16. Wang, F.; Itkis, M. E.; Bekyarova, E.; Haddon, R. C. *Nature Photon.* **2013,** 7, 459-465.

17. Bao, Q.; Loh, K. P. *ACS Nano* **2012,** 6, 3677-3694.

18. Polat, E. O.; Balci, O.; Kocabas, C. *Sci. Rep.* **2014,** 4, 6484.

19. Shimotani, H.; Tsuda, S.; Yuan, H.; Yomogida, Y.; Moriya, R.; Takenobu, T.; Yanagi, K.; Iwasa, Y. *Adv. Funct. Mater.* **2014,** 24, 3305-3311.

20. Fujimoto, T.; Awaga, K. *Phys Chem Chem Phys* **2013,** 15, 8983-9006.

21. Yanagi, K.; Moriya, R.; Yomogida, Y.; Takenobu, T.; Naitoh, Y.; Ishida, T.; Kataura, H.; Matsuda, K.; Maniwa, Y. *Adv. Mater.* **2011,** 23, 2811-2814.

22. Collins, P. G.; Bradley, K.; Ishigami, M.; Zettl, A. *Science* **2000,** 287, 1801-1804.

23. Bockris, J. O. M.; Reddy, A. K. N., *Modern Electrochemistry 1. Ionics*. Second ed.; Plenum Publishing Corporation: N. Y. N. Y., 1998; Vol. 1, p 767.

24. Bard, A. J.; Faulkner, L. R., *Electrochemical Methods. Fundamental and Applications*. Second ed.; John Wiley & Sons, Inc.: N. Y. N. Y., 2001; p 833.

25. Nair, R. R.; Blake, P.; Grigorenko, A. N.; Novoselov, K. S.; Booth, T. J.; Stauber, T.; Peres, N. M. R.; Geim, A. K. *Science* **2008,** 320, 1308.

26. Bonaccorso, F.; Sun, Z.; Hasan, T.; Ferrari, A. C. *Nature Photon.* **2010,** 4, 611-622.

27. http:/www.lc-tec.se.

28. Itkis, M. E.; Niyogi, S.; Meng, M.; Hamon, M.; Hu, H.; Haddon, R. C. *Nano Lett.* **2002,** 2, 155-159.

Chapter 5. Conclusions and Future Outlook

Single-walled carbon nanotubes (SWNTs), a low dimensional carbon allotrope, continue to attract strong interest due to their unique electronic properties and wide applications. The ability to interconnect and enhance the electronic structures of SWNT by single atom covalent / ionic bonds (atomtronics), allows this material to be considered for applications such as catalysis, high mobility transistor, spintronic and memory devices.

An exciting new phenomena has been discovered, exemplified by the formation of a bis-hexahapto-metal bond with ionic character. The mode of bonding between adjacent benzenoid rings of graphitic surfaces largely preserves the band structure and π-conjugation, resulting in the enhancement of conductivity due to the increased dimensionality of the electronic structure. These atomic, chemically formed “electron bridges” are entirely distinct from other modes that depend on the adsorption of bulk materials.

The Ln(η^6-SWNT)$_2$ complexes offer a new type of carbon-lanthanide bond stability and establishes the nanotube walls as excellent ligands in bis-hexahapto coordination. The conductivity of these complexes highlights this form of linkage to seamlessly interconnect the conjugated carbons of the SWNTs and extend their dimensionality. The greatly enhanced conductivity of both Sm(η^6-SWNT)$_2$ and

Eu(η^6-SWNT)$_2$ validates the idea that this form of nanotube film exhibits the first known instances of mixed covalent-ionic bonding in bis-hexahapto complexes.

This newly discovered interaction has promise of new ferromagnetic and superconducting materials that are based on the other types of known systems seen in organometallic graphite and C_{60} intercalation compounds, and would lead to self-assembled metal nanoclusters, 3D electronics based on 1D SWNTs or 2D graphene structures (atomtronics), architectures for novel catalyst, and organometallic transistor devices. This is a new fertile area of science and technology where we can expect more fascinating results to come about soon.

In our other development, an ionic liquid gated infrared modulator composed of a SWNT active electrode was designed and tested to determine the optical characteristics and effectiveness of using SWNTs in electrochromic reversible doping devices. When paired with a MT-SWNT thin film as the transparent counter-electrode the effect was a fast operating, strong modulating system that performed better than known devices. Comparing similar devices with various active electrode thicknesses and sampling different types of counter-electrode material, device optimization lead to a system with a modulation depth of 6.7 dB and incredibly fast on/off response of a few milliseconds. The outstanding performance of the SWNT based electrochromic cell was a result of the nanotube films high porosity and high surface area, in which fast penetration of the ions allowed the formation of a 3-dimensional electric double layer (EDL) capacitor

down to the bottom of the film and encompassed the entire thin film surface area. This was why enhanced modulation was found when MT-SWNT film was used as counter electrode and not seen when a more conductive graphene sheet was used in its place. Following these results, a dual sided active electrode electro-optical modulator was designed and tested, where both electrodes consisted of the electro-optically active (SC-SWNT) material and showed an enhanced modulation depth with millisecond response time, with a capability to generate a second harmonic response.

Electrochromic device consisting of a SC-SWNT active electrode and a MT-SWNT counter electrode provides an opportunity to break open the field of thin film SWNT devices for optoelectronics and creates areas for potential applications in smart windows, infrared modulators and short wave infrared imagers. The field of SWNT optoelectronic modulators is relatively new forming within the last decade. There is a lot of SWNT materials that could potentially open the active optical region to both sides of short-wave infrared wavelengths that was investigated in this study. By changing substrate materials, testing could be carried out into the 8-14 μm long-wavelength regions and could bear similar results as seen in the device discussed earlier. Using SWNTs of different diameters could find that very fast optical modulation is possible in the visible and near-infrared spectral regions. Findings such as those would open the door for more of real world applications.